Published in final edited form as:
Eur J Med Chem. 2009 February ; 44(2): 593–608. doi:10.1016/j.ejmech.2008.03.040.

Analogs of JHU75528, a PET ligand for imaging of cerebral cannabinoid receptors (CB1): development of ligands with optimized lipophilicity and binding affinity

Hong Fan[†], **Evangelia Kotsikorou**[‡], **Alexander F. Hoffman**[◆], **Hayden T. Ravert**[†], **Daniel Holt**[†], **Dow P. Hurst**[‡], **Carl R. Lupica**[◆], **Patricia H. Reggio**[‡], **Robert F. Dannals**[†], and **Andrew G. Horti**[†,*]

[†] Division of Nuclear Medicine, Department of Radiology, Johns Hopkins University School of Medicine, Baltimore, MD 21287 U.S.A

[‡] Center for Drug Discovery, Chemistry and Biochemistry Department, University of North Carolina, Greensboro, NC 27402-6170 USA

[◆] United States Department of Health and Human Services, National Institutes of Health, National Institute on Drug Abuse Intramural Research Program, Cellular Neurobiology Branch, Electrophysiology Research Unit, Baltimore MD 21224 U.S.A

Abstract

Cyano analogs of Rimonabant with high binding affinity for the cerebral cannabinoid receptor (CB1) and with optimized lipophilicity have been synthesized as potential positron emission tomography (PET) ligands. The best ligands of the series are optimal targets for the future radiolabeling with PET isotopes and in vivo evaluation as radioligands with enhanced properties for PET imaging of CB1 receptors in human subjects. Extracellular electrophysiological recordings in rodent brain slices demonstrated that JHU75528, **4**, the lead compound of the new series, has functional CB antagonist properties that are consistent with its structural relationship to Rimonabant. Molecular modeling analysis revealed an important role of the binding of the cyano-group with the CB1 binding pocket.

Keywords

cannabinoid receptor; carbon-11; JHU75528; Rimonabant; Positron Emission Tomography; molecular modeling; receptor docking

1. Introduction

To date, at least two subtypes of the cannabinoid receptor, CB1 and CB2, have been cloned. [1] CB1 receptors are located predominantly in the brain and to a lesser extent in ganglionic system whereas CB2 receptors are found mainly on immune cells[1] and, in low density, in the brain.[2] The currently known classes of cannabinoid receptor ligands (see for review[3]) include tetrahydrocannabinol (Δ^9-THC), the principal psychoactive constituent in marijuana

*Corresponding author: Phone: 410-614-5130; Email address: ahorti1@jhmi.edu; Address: PET Center, Division of Nuclear Medicine, Radiology, Johns Hopkins Medicine, 600 North Wolfe Street, Nelson B1-122, Baltimore, MD 21287-0816 USA.

(*Cannabis sativa L.*), the nonclassical cannabinoids including (−)-CP-55940, the endogenous cannabinoid ligand anandamide and its analogs, the aminoalkylindoles (WIN 55212-2), and cannabinoid antagonists. The most representative member of the latter class is Rimonabant (Acomplia™ or SR-141716) **1** (Fig 1) which is a first highly selective CB1 antagonist developed by Sanofi-Aventis.[4] Rimonabant **1** was granted authorization for marketing in European Union states in 2006 as an anti-obesity drug.[5,6] Cannabinoid ligands and, particularly, CB1 antagonists are an emerging class of drugs for control of appetite,[5–8] treatment of neuropsychiatric disorders,[9–13] and drug dependence.[14–16] In addition, there is a growing number of structurally diverse CB1 antagonists/inverse agonists[17] that possess a pharmacophoric arrangement similar to that of **1**.

The ability to image CB1 receptors in the human brain using positron emission tomography (PET) or single photon emission computed tomography (SPECT) would provide the possibility to conduct non-invasive receptor studies under normal physiological conditions and in disease states. The development of useful PET radiotracer would assist in the design and testing of promising pharmaceuticals targeting the CB1 receptor.

Initial attempts by several groups to image CB1 in animal brains examined the feasibility of specific labeling of CB1 in vivo.[18–28] Unfortunately, all of the radioligands initially studied (more than 10; mostly analogues of Δ^9-tetrahydrocannabinol, the principal psychoactive component of marijuana, cannabinoid agonist WIN 55212-2 and **1**) exhibited insufficient properties for quantification of CB1 receptor by PET (low specific binding, high non-specific binding and/or low brain uptake). The attempts to quantify CB1 in the living human brain by SPECT and PET demonstrated low binding potential (BP=0.21 and 0.37) for the radioligands [^{123}I]**2**[27] and [^{124}I]**2**[28], correspondingly (Fig. 1). High lipophilicity and tight association to proteins were likely causes of high non-specific binding that resulted in low contrast of the in vivo images with labeled **2**.[27,28] Compound [^{11}C]**3** (Fig 1) synthesized by our group in the past[21,29] also displayed a low BP (0.6) and relatively low brain uptake in the Rhesus monkey brain due to its high lipophilicity and moderate binding affinity.[29,30]

Recently we reported development of JHU75528 **4** (Fig 2, Table 1), an analog of Rimonabant having a combination of greater CB1 in vitro binding affinity and lower lipophilicity than those of the previously studied CB1 in vivo radioligands.[31] Compound [^{11}C]**4** is the first CB1 PET radioligand manifesting reasonable imaging properties in animals[32] and human PET studies with [^{11}C]**4** is currently in progress. New reports of other groups described the development of [^{11}C]Me-PPEP ([^{11}C]**5**)[33] and [^{18}F]MK-9470 ([^{18}F]**6**)[34] (Fig 2) that are also suitable for quantitative PET imaging of CB1 radioligands. Yet, PET imaging properties of all three compounds[32–34] are not ideal and exhibit certain drawbacks including modest binding potential and/or moderate brain uptake and/or slow brain kinetics. Thus, the binding potentials of all three compounds [^{11}C]**4**, [^{11}C]**5** and [^{18}F]**6** are moderate.[32–34] However, unlike the case with [^{11}C]**5** and [^{18}F]**6**[33,34] having very slow brain kinetics the radioligand [^{11}C]**4** manifests ideal brain kinetics in non-human primate studies for PET quantification.[32] We suggested that improvement of imaging properties of [^{11}C]**4** including binding potential and total brain uptake could be achieved by development of analogs of [^{11}C]**4** with better in vitro properties: higher binding affinity and reduced lipophilicity within the optimal range for PET radioligands (logD = 1–3). Here we are presenting a series of analogs of **4** with improved binding affinity and lipophilicity.

2. Results and Discussion

Chemistry

Novel analogs of **4** (compounds **7a-i**) were synthesized in this study *via* the general methods described in the industrial patent[35] and our paper[31] using three building blocks: derivatives

of benzoylacetonitrile **8**, derivatives of ethyl 2-chloro-2-(2-benzylhydrazono)acetate **9** and cyclic 1,1-dialkylhydrazines **10** (Scheme 1, 2).

Ethyl 2-chloro-2-(2-benzylhydrazono)acetates **9a** and **9b** (Scheme 1) were obtained in two steps by conversion of corresponding commercially available anilines **11a** and **11b** into arenediazonium salts followed by reaction with ethyl 2-chloro-acetoacetate using the previously published method.[36] The intermediate benzoylacetonitrile **8a** was prepared by reaction of ethyl 4-iodobenzoate with acetonitrile in the presence of sodium ethoxide [37] (Scheme 1).

The cycloaddition (Scheme 1) of benzoylacetonitriles **8a–8c** and ethyl 2-chloro-2-(2-benzylhydrazono)acetates derivatives **9a–9d** in the presence of sodium ethoxide yielded ethyl 4-cyano-1,5-diaryl-1H-pyrazole-3-carboxylates **12a–12e**. Under the conditions of this reaction, the cyano-group can undergo a side reaction yielding the corresponding 4-carbamoylpyrazole as a by-product. Thus, ethyl 1-(2-bromophenyl)-4-carbamoyl-5-(4-methoxyphenyl)-1H-pyrazole-3-carboxylate **12e′** was obtained as a major by-product of ethyl 1-(2-bromophenyl)-4-cyano-5-(4-methoxyphenyl)-1H-pyrazole-3-carboxylate **12e** that is described elsewhere[31].

The ethyl esters **12a–12d, 12e′** were saponified with lithium hydroxide (Scheme 2) to give the carboxylic acids **13a–13e** that were further coupled with either 1-aminopiperidine **10a**, 1-aminopyrrolidine **10b** or 1-aminomorpholine **10c** in the presence of benzotriazol-1-yloxytris (dimethylamino)-phosphonium hexafluorophosphate (BOP) to produce **7a–7h** in reasonable yields.

The fluoromethoxy derivative **7i** was prepared by fluoromethylation of the corresponding phenol **14**[31]with fluoromethyl tosylate[38] (Scheme 3)

Structure-activity relationships

The overall objective of this study is in development of analogs of **4** with reduced lipophilicity and improved binding affinity as potential PET ligands for imaging CB1 receptor. In our previous structure-activity relationship study with derivatives of Rimonabant **1** replacement of a lipophilic substituent attached to the C5 benzene ring of **1** with a substituent with reduced hydrophobic constant π led to a reduction in binding affinity whereas there was no clear correlation of the binding affinity *vs*. hydrophobic properties of the substituents of the N1 benzene ring.[29,30] Therefore, here we have initially chosen to replace the chloro substituents of N1-benzene ring of **4**. Replacement of the 4-chloro substituent with fluorine gave the chloro-fluoro derivative **7a** with comparable binding affinity and reduced lipophilicity (Table 1). When both chlorine atoms of **4** were replaced with fluorine and bromine, derivative **7b** with lower binding affinity (Table 1) was obtained.

Reduction of the number of C-atoms in the molecule usually reduces a compound lipophilicity. Shrinkage of the piperidine ring of **4** to a pyrrolidine ring revealed analog **7h** with lower lipophilicity and slightly higher binding affinity. The previous studies did not demonstrate an improvement of the binding affinity of pyrrolidinyl *vs*. piperidinyl analogs in the **5** series. [40]

Conversion of the methoxy-group of **4** to the fluoromethoxy-group gave an equally potent CB1 ligand **7i** with reduced lipophilicity.

It is noteworthy that replacement of the 4-cyano group of the high affinity ligand **15**[31] (Table 1) with 4-carbamoyl group yielded derivative **7e** that did not bind with the CB1 receptor. This finding is disappointing because compound **7e** manifests a lipophilicity value in the target range

(Table 1). The binding affinity matter of **7e** is discussed in greater details below in the molecular modeling section.

Radioligands [^{123}I]**2** and [^{124}I]**2** (Fig 1), radioiodinated analogs of **1**, were developed as SPECT and PET ligands for studying CB1 receptors in human subjects.[27,28] We hypothesized that replacement of the 4-methyl group in the molecule **2** with a cyano substituent might give a better ligand. As we expected, the binding affinity of the 4-cyano compound **7f** was greater than that of **2** (Table 1). Compound **7c,** a piperidinyl analog of the morpholinyl derivative **7f**, manifested even better binding affinity but, also, substantially higher lipophilicity than that of **7f**. Surprisingly, brominated ligand **7d** shows an improved binding affinity as compared with its iodinated congener **7c**. Previous SAR studies with 4-Br and 4-I analogs of **1** demonstrated a higher binding affinity of the iodo derivative.[40]

Replacement of the 4-methyl group in **1** with a 4-cyano group yielded compound **7j** previously described in an industrial patent.[35] The binding affinity of **7j** was not reported in the patent. Experimental determination of properties of **7j** demonstrated that this CN-analog of **1** displays higher binding affinity and lower lipophilicity than those of **1** (Table 1). The role of the cyano group on the binding with CB1 receptor is discussed below.

Good binding affinity and reduced lipophilicity of **7a**, **7h** and **7i** suggest that if radiolabeled with positron-emitting isotopes ^{11}C and ^{18}F these ligands might be better than [^{11}C]**4** as PET radioligands.

Molecular Modeling Studies—The goal of modeling studies was to assess if the cyano compound **4** could occupy the same binding site at CB1 receptor as the methylated lead compound **1** and to probe the CB1 receptor state model for the molecular origins of the low binding affinity of compound **7e.** Our previous combined mutation/modeling studies suggested that the binding site of the CB1 inverse agonist/antagonist, **1**, is within the transmembrane helix (TMH)3-4-5-6 aromatic microdomain and involves direct aromatic stacking interactions with F3.36(200), Y5.39(275), and W5.43(279).[41] Our modeling studies also suggested that although **1** can engage in aromatic stacking interactions in the inactive (R) and active (R*) states of CB1, the C3 substituent carboxamide oxygen of **1** can hydrogen bond with K3.28 (192) only in the CB1 inactive (R) state.[42] Through mutant cycle[42] and SAR studies,[43] we have demonstrated that the inverse agonism produced by **1** is likely due to this hydrogen bonding interaction with K3.28(192).

Conformational Analysis—The global minimum energy conformer of **4** (see Figure 3) has the carboxamide oxygen of the C3 substituent nearly in plane with the pyrazole ring and pointing in the direction of the C4 cyano group (O-C1′-C3-C4= 2.3°). The piperidine ring is in a chair conformation with the lone pair of the nitrogen electrons pointing in the same direction as the carboxamide hydrogen (LP-N3′-N2′-H= −1.0°). The C5 substituent para-methoxy ring is out of plane with the pyrazole ring (C4-C5-C1‴-C2‴ = −47.3°) and the methoxy group is nearly in the plane of the aromatic ring (C3‴-C4‴-O-C= 3.3 °). The N1 substituent dichlorophenyl ring is also out of plane with the pyrazole ring (N2-N1-C1″-C2″= −74.7°). In this position the *ortho*-chloro is in the bottom face of the molecule. This conformation is very similar to the previously calculated global minimum energy conformer of SR141716A (5) [42],[43] (see Figure 3).

The global minimum energy conformer of **7e** (see Figure 3) has the carboxamide oxygen of the C3 substituent slightly out of plane with the pyrazole ring and pointing in the direction of the C4 amide group (O-C1′-C3-C4= −5.5°). The piperidine ring is in a chair conformation with the lone pair of the nitrogen electrons pointing in the same direction as the carboxamide hydrogen (LP-N3′-N2′-H= −1.7°). The C5 substituent para-methoxy ring is out of plane with

the pyrazole ring (C4-C5-C1‴-C2‴ = −55.6°) and the methoxy group is nearly in the plane of the aromatic ring (C3‴-C4‴-O-C= 3.2°). The N1 substituent bromophenyl ring is also out of plane with the pyrazole ring (N2-N1-C1″-C2″= −71.9°). In this position, the *ortho*-bromo is in the bottom face of the molecule. **7e** also has an intramolecular hydrogen bond that locks the position of the carboxamide oxygen of the C3 substituent and the amide nitrogen of the C4 substituent in place. The hydrogen bond distance (N--O) and angle (N-H-O) are 2.70 Å and 156.0° respectively.

CB1 Receptor State Model Docking Studies—Based on our recent paper,[43] we docked in our model of the CB1 inactive (R) state, a minimum energy conformer of **4** in which the lone pair of electrons of the piperidine nitrogen points in the direction opposite to the carboxamide hydrogen (see Figure 4 and also Tables A1 and A2 in appendix for further information). Modeling studies revealed that compound **4** can occupy a similar orientation within the CB1 R binding pocket as SR141716 (**1**). The energy minimized ligand/CB1 inactive (R) state complexes for **4** and **1**[43] are illustrated in Figure 4. In Figure 4(**A**), Compound **4** is docked in a minimum energy conformation (ΔE= 1.25 kcal/mol above its global min) in the CB1 inactive state TMH3-4-5-6 aromatic microdomain region. In Figure 4(B), SR141716 (**1**) is docked in the same TMH3-4-5-6 aromatic microdomain in a minimum energy conformation (ΔE= 0.92 kcal/mol above its global min). [42],[43] The view in Figure 4 is from lipid, looking towards TMHs 3 and 4. TMHs 1, 2 and 7 are not shown in order to simplify the view. Aromatic residues for which **4** and **1** have a direct aromatic stacking interaction are colored orange here. Aromatic residues that are part of the extended aromatic cluster are colored yellow, while those that are not part of the aromatic cluster are colored cyan. In Figure 4(**A**), both the carboxamide oxygen (N--O = 2.65Å, N-H –O= 157°) and the cyano group of **4** (N- -N=2.81Å, N-H–N=122°) have hydrogen-bonding interactions with K3.28(192), a residue that is part of a K3.28(192)/D6.58(366) salt bridge that is a characteristic of the R state model.[43] **4** directly stacks with W5.43(279) (methoxy ring d=4.9Å and α=85°, dichloro (DC) ring d=4.6Å and α= 78°) and F3.36(200) (DC ring d=5.1Å and α=83°). While the C5 substituent para-methoxy ring cannot have a direct aromatic stacking interaction with Y5.39(275) due to the intervening methoxy group, this substituent does have a strong interaction with Y5.39(275) (see Table A3). In this way, the ligand acts as a bridge between the F3.36(200)/W5.43(279)/W6.48(356) and Y5.39(275)/W4.64(255)/F5.42(278) aromatic clusters present in the TMH3-4-5-6 aromatic microdomain in the minimized complex. In Figure 4(**B**), the carboxamide oxygen of **1** (N--O = 2.65Å, N-H –O= 156°) has a hydrogen-bonding interaction with K3.28(192) in the K3.28(192)/D6.58(366) salt bridge. Compound **1** has direct aromatic stacking interactions with F3.36(200) (monochloro (MC) ring d=6.9Å and α=56°, DC ring d=5.3Å and α=65°) and W5.43(279) (MC ring d=4.7Å and α=44°, DC ring d=5.2Å and α=86°) and with Y5.39(275) (MC ring d=6.0Å and α=60°) bridging the F3.36(200)/W5.43(279)/W6.48(356) and Y5.39(275)/W4.64(255)/F5.42(278) aromatic clusters and forming one large extended cluster in the minimized complex.

The pairwise interaction energy analysis of the **4**/CB1 R and **1**/CB1 R complexes revealed that the greatest coulombic interactions for **4** (−92.84 kJ/mol) and **1** (−72.02 kJ/mol) were with K3.28. The greater coloumbic interactions for **4** reflect the fact that this compound forms two hydrogen bonds with K3.28, while **1** forms one hydrogen bond. High van der Waals' interactions were found for both ligands with W5.43 (**4**, −29.34 kJ/mol; **1**, −25.10 kJ/mol) and with M6.55 (**4**, −32.22 kJ/mol; **1**, −28.36 kJ/mol). In addition, **4** was found to have a strong van der Waals interaction with D6.58(366) (−15.72 kJ/mol) and **1** with V3.32(196) (−20.29 kJ/mol). A table that includes all of the calculated pairwise interaction energies for **4** and **1** at CB1 R is included in the Appendix here (Table A3). The fact that the combined total energy of pair-wise interaction is lower for **4** (−261.90 kJ/mol or −62.55 kcal/mol)) than for **1** (−218.63 kJ/mol or −52.22 kcal/mol), may be the reason why **4** has higher CB1 affinity than **1**. It is important to note, however, that pair-wise interaction energies may not be directly comparable

with changes in affinities. The experimentally measured change in affinity includes not only the strength of ligand-receptor interactions in the newly formed complex, but also the possible loss of intrareceptor interactions in the unoccupied receptor resulting from ligand binding. While Table A3 should reflect the former, it does not take into consideration the latter.

Compound **7e** has a K_i> 10,000 nM at CB1 (see Table 1). Figure 5 illustrates that when this compound is docked in the same CB1 R TMH3-4-5-6 aromatic microdomain binding site as **1** and **4,** it exceeds the steric limitations of this site in nearly every direction. The most severe steric clash results from the substitution of the amide group for the cyano group at C4 in **4**. This produces a severe steric clash between the C4 substituent amide nitrogen of **7e** and residues K3.28(192) and D6.58(366), as well as a clash between the C4 carboxamide oxygen and residue L3.29(193). A severe steric clash also exists between the **7e** piperidine ring and residues C7.42 (386) and S7.39(383), as well as between the methoxy group of the C5 substituent para-methoxyphenyl ring and residues Y5.39(275) and W5.43(279). Finally, there is a steric clash between the bromine of the **7e** N1 substituent ortho-bromophenyl ring and residue V3.32(196) (not shown in Figure 5) and the phenyl ring of the **7e** N1 substituent ortho-bromophenyl ring and residue M6.55(363).

Functional assay

Given the structural similarity of the series that include **4** and its analogs (Table 1) to the antagonist **1**, we wondered if any of these compounds might functionally reverse the actions of the known CB agonist WIN 55212-2. Extracellular electrophysiological recordings were performed in rodent brain slices containing the striatum and nucleus accumbens. In this preparation, glutamatergic field potentials are known to be inhibited by CB agonists via presynaptic activation of CB1 receptors.[44,45] Bath application of 1 μM WIN 55212-2 inhibited glutamate release by ~30% (Fig 6). When 3 μM **4** was applied subsequent to WIN 55212-2, this inhibitory effect was rapidly reversed. These data demonstrate that **4** exhibits functional CB antagonist properties, consistent with its structural relationship to **1**.

Cannabinoid antagonists have an advantage over agonists for *in vivo* imaging of CB1 receptors because antagonists bind to a greater population of the receptor than agonists do.[24,46] Therefore, if all other properties are the same, the BP value of a radiolabeled CB1 antagonist will be greater than that of a radiolabeled agonist. In addition, the side effects of CB1 antagonists in vivo are lower. Perhaps the antagonistic properties of [^{11}C]**4** is one of the reasons for its success in the animal imaging experiments.[32]

Radiochemistry and in vivo studies—Having the best combination of high in vitro binding affinity and lowest lipophilicity (Table 1), compound **7h** was labeled with [^{11}C]methyl triflate by radiomethylation of corresponding phenol precursor **16** (Scheme 4). After purification and formulation the radiochemical yield of [^{11}C]**7h** was 15–24%, specific radioactivity was 482±288 GBq/μmol (13019±7800 mCi/μmol) and radiochemical purity was 98%. The precursor **16** was synthesized via the carboxylic acid **17**[31] and the intermediate **18** (Scheme 5).

The preliminary in vivo evaluation of [^{11}C]**7h** was performed in CD-1 mice. We also performed regional brain distribution studies in mice with 1-(2-bromophenyl)-4-cyano-5-(4-[^{11}C] methoxyphenyl)-N-(piperidin-1-yl)-1H-pyrazole-3-carboxamide ([^{11}C]JHU75575) [^{11}C]**15**, a monobromo analog of **4** that we synthesized in the past[31] (Table 1).

The mouse brain uptake of [^{11}C]**7h** and [^{11}C]**15** was quite high (Fig 7) and comparable with previously studied [^{11}C]**4** ([^{11}C]JHU75528[32]). The highest accumulation of ^{11}C radioactivity occurred in the hippocampus, frontal cortex and cerebellum and lowest radioactivity was seen in the brainstem. This distribution of radioactivity of [^{11}C]**7h** and [^{11}C]

15 in the mouse brain matches the data obtained in the previous autoradiographic studies[47] and distribution of [^{11}C]**4.**[32] The clearance rates of [^{11}C]**7h** and [^{11}C]**15** from the brainstem were higher than from any other region studied. The hippocampus-to-brainstem ratio of [^{11}C]**7h** was greater than that of [^{11}C]**15** and reached values of 2.3, 3.0 and 3.5 at 30, 45 and 90 min post injection, correspondingly. These target-to-non-target ratios are the highest reported to date and are 10–30% greater of those previously obtained for [^{11}C]**4.**[32] The superior ratio of [^{11}C]**7h** *versus* [^{11}C]**4**[32] or [^{11}C]**15** is in agreement with better combination of binding affinity and lower lipophilicity of [^{11}C]**7h** (Table 1).

A blocking dose of the selective CB1 antagonist **1** significantly inhibited [^{11}C]**7h** binding at 60 min after administration of the radiotracer in the hippocampus, a region with highest density of CB1 receptors, but it failed to significantly block accumulation of radioactivity in the brainstem, a region with a low density of CB1 (Fig. 8). This study demonstrated that uptake of [^{11}C]**7h** in the receptor-rich hippocampus is CB1-mediated.

3. Conclusion

A novel series of analogs of JHU75528 **4** with high affinity for CB1 receptor and reduced lipophilicity has been synthesized. Given the excellent in vitro properties of the best compounds of the series (**7a**, **7h** and **7i)**, these are the targets for the future evaluation as potential radioligands with enhanced properties for PET imaging of CB1 receptors in human subjects. Preliminary evaluation of [^{11}C]**7h** in the mouse brain demonstrated a better target-to-non-target ratio of [^{11}C]**7h** than that of [^{11}C]**4** and [^{11}C]**15**.

Compound **4**, the lead of the series described here, displays a higher binding affinity than that of its congener Rimonabant **1**. This finding is in agreement with the conformational analysis and CB1 receptor docking studies that demonstrated that even though **4** has a similar binding arrangement as **1**, the former forms an additional hydrogen bond between the cyano group with the K3.28(192)/D6.58(366) salt bridge. Replacement of 4-cyano group with 4-carbamoyl group in the molecule **7e** led to severe steric clash between amide nitrogen and piperidine ring and the receptor binding site. This finding is in agreement with very low CB1 binding affinity of **7e**.

Extracellular electrophysiological recordings in rodent brain slices demonstrated that **4**, the lead compound of the new series and potential PET radioligand for imaging of CB1 receptors in humans, has functional CB antagonist properties, consistent with its structural relationship to Rimonabant **1**.

4. Experimental Protocols

4.1 General

All chemicals and solvents were reagent grade, and were used as received from Aldrich. ^{1}H NMR spectra were obtained with a Varian 400 MHz spectrometer. Chemical shifts are reported in ppm (δ) relative to internal tetramethylsilane in $CDCl_3$. High resolution mass spectrometry was performed at the University of Notre Dame Mass Spectrometry Facility. Galbraith Laboratories Inc. (Knoxville, TN) did elemental analysis. Flash chromatography purification was performed using E. Merck 7729 (<230 mesh) silica gel. All HPLC chromatograms were recorded by a Varian Galaxie system. Semi-preparative (10 mm × 300 mm) and analytical (4.6 mm × 100 mm) 10 μM C18 Luna columns (Phenomenex Torrance, CA) were used for purification and quality control, respectively.

4.2. 3-(4-Iodophenyl)-3-oxopropanenitrile (8a)

A mixture of ethyl 4-iodobenzoate (2.76 g, 10 mmol), NaOEt (0.748 g, 11 mmol), and acetonitrile (0.65 mL, 12 mmol) in anhydrous toluene (5 mL) was stirred at 110 °C for 20 h. The reaction mixture was cooled and diluted with 30 mL water to dissolve solids. The mixture was washed with Et_2O (2×30 mL). The aqueous layer was acidified with 1N HCl to pH 7, and then was extracted with CH_2Cl_2 (3×30 mL), washed with brine and dried over Na_2SO_4. The organic solvent was removed and the desired product **8a** was obtained (980 mg, 36%). ^{1}H NMR ($CDCl_3$, δ) 4.04 (s, 2H, CH2), 7.63 (d, *J* = 8.0 Hz, 2H, ArH), 7.91 (d, *J* = 8.0 Hz, 2H, ArH). FAB-HRMS: calcd. for C_9H_6INO: 270.9494; found: 271.9590 $(M+H)^+$.

4.3. Chloro[(2-chloro-4-fluorophenyl)hydrazono]ethyl acetate (9a)

A mixture of 2-chloro-4-fluoroaniline **11a** (3.22 g, 22.5 mmol) in 37.5 mL 24% HCl, and 100 mL water was stirred for 2 h at room temperature. The reaction mixture was cooled with ice and a solution of sodium nitrite (1.59 g, 23 mmol) in 11 mL water was added dropwised for 30 min. The mixture was then added to a solution of sodium acetate (1.76 g, 21.5 mmol) and ethyl 2-chloro-acetoacetate (3.11 mL, 22.5 mmol) in 225 mL EtOH, and cooled with ice. The temperature was allowed to increase slowly for 2 h. The precipitate was filtered and washed with water and dried to give the desired product 4.79 g, (76%). ^{1}H NMR ($CDCl_3$, δ) 1.41 (t, *J* = 6.8 Hz, 3H, CH_3), 4.40 (q, *J* = 6.8 Hz, 2H, CH_2), 7.03 (m, 1H, ArH), 7.12 (dd, J_1 = 7.6 Hz, J_2 = 2.4 Hz, 1H, ArH), 7.59 (m, 1H, ArH), 8.69 (b, 1H, NH).

4.4. Chloro[(2-bromo-4-fluorophenyl)hydrazono]ethyl acetate (9b)

Compound **9b** was prepared from 2-bromo-4-fluoroaniline **11b** with the same procedure described for **9a**. Yield was 66%. ^{1}H NMR ($CDCl_3$, δ) 1.41 (t, *J* = 6.8 Hz, 3H, CH_3), 4.40 (q, *J* = 6.8 Hz, 2H, CH_2), 7.08 (m, 1H, ArH), 7.28 (dd, J_1 = 8.0 Hz, J_2 = 2.8 Hz, 1H, ArH), 7.58 (m, 1H, ArH), 8.73 (b, 1H, NH).

4.5. Ethyl 1-(2-chloro-4-fluorophenyl)-4-cyano-5-(4-methoxyphenyl)-*1H*-pyrazole-3-carboxylate (12a)

A mixture of chloro[(2-chloro-4-fluorophenyl)hydrazono]ethyl acetate **9a** (1.53 g, 5.5 mmol), 4-methoxybezoylacetonitrile **8c** (0.97g, 5.5 mmol), 60 mL EtOH, and sodium ethoxide, that was prepared by dissolving 0.14 g sodium in 12.5 mL EtOH, was heated to reflux for 18 h and solvent was evaporated under reduced pressure. Ethyl acetate (75 mL) was added and the precipitate was filtered. The organic layer was washed with water and saturated NaCl. The residue was purified by flash chromatography (silica gel, 10:90 EtOAc/hexane to 50:50 EtOAc/CH_2Cl_2) to afford the desired product. Yield: 155 mg (7 %). ^{1}H NMR ($CDCl_3$, δ) 1.45 (t, *J* = 7.2 Hz, 3H, CH_3), 3.81 (s, 3H, OCH_3), 4.53 (q, *J* = 6.8 Hz, 2H, CH_2), 6.86 (d, *J* = 8.8 Hz, 2H, ArH), 7.11 (m, 1H, ArH), 7.19 (m, 1H, ArH), 7.28 (d, *J* = 8.8 Hz, 2H, ArH), 7.48 (m, 1H, ArH). FAB-HRMS: calcd. for $C_{20}H_{15}ClFN_3O_3$: 399.0786; found: 399.0777.

4.6. Ethyl 1-(2-bromo-4-fluorophenyl)-4-cyano-5-(4-methoxyphenyl)-*1H*-pyrazole-3-carboxylate (12b)

Compound **12b** was prepared from chloro[(2-bromo-4-fluorophenyl)hydrazono]ethyl acetate (**9b**) with the same procedure described for **12a**. Yield was 10 %. ^{1}H NMR ($CDCl_3$, δ) 1.47 (t, *J* = 7.2 Hz, 3H, CH_3), 3.81 (s, 3H, OCH_3), 4.52 (q, *J* = 7.2 Hz, 2H, CH_2), 6.88 (d, *J* = 8.4 Hz, 2H, ArH), 7.15 (m, 1H, ArH), 7.26 (d, *J* = 8.8 Hz, 2H, ArH), 7.36 (m, 1H, ArH), 7.46 (m, 1H, ArH). FAB-HRMS: calcd. for $C_{20}H_{15}BrFN_3O_3$: 443.0281; found: 443.0287.

4.7. Ethyl 1-(2,4-dichlorophenyl)-4-cyano-5-(4-iodophenyl)-*1H*-pyrazole-3-carboxylate (12c)

Compound **12c** was prepared from ethyl chloro[(2,4-dichlorophenyl)hydrazono]acetate **9d** [35] and 3-(4-iodophenyl)-3-oxopropanenitrile **8a** with the same procedure described for **12a**. Yield was 25%. ^{1}H NMR ($CDCl_3$,δ) 1.47 (t, J = 6.8 Hz, 3H, CH_3), 4.53 (q, J = 1.2 Hz, 2H, CH_2), 7.04 (d, J = 8.8 Hz, 2H, ArH), 7.39–7.47 (m, 3H, ArH), 7.75 (d, J = 7.6 Hz, 2H, ArH). FAB-HRMS: calcd. for $C_{19}H_{12}Cl_2IN_3O_2$: 510.9351; found: 511.9435 $(M+H)^+$.

4.8. Ethyl 1-(2,4-dichlorophenyl)-4-cyano-5-(4-bromophenyl)-*1H*-pyrazole-3-carboxylate (12d)

Compound **12d** was prepared from ethyl chloro[(2,4-dichlorophenyl)hydrazono]acetate **9d** [35] and commercially available 3-(4-bromophenyl)-3-oxopropanenitrile **8b** with the same procedure described for **12a**. Yield was 41 %. ^{1}H NMR ($CDCl_3$, δ) 1.47 (t, J = 6.8 Hz, 3H, CH_3), 4.52 (q, J = 6.8 Hz, 2H, CH_2), 7.19 (d, J = 8.4 Hz, 2H, ArH), 7.39–7.47 (m, 3H, ArH), 7.54 (d, J = 8.4 Hz, 2H, ArH). FAB-HRMS: calcd. for $C_{19}H_{12}BrCl_2N_3O_2$: 462.9490; found: 463.9588 $(M+H)^+$.

4.9. Ethyl 1-(2-bromophenyl)-4-carbamoyl-5-(4-methoxyphenyl)-*1H*-pyrazole-3-carboxylate (12e′)

A mixture of chloro[(2-bromophenyl)hydrazono]ethyl acetate **9c**[31] (1.63 g, 5.5 mmol), 4-methoxybezoylacetonitrile **8c** (0.97 g, 5.5 mol), 60 mL EtOH, and sodium ethoxide, which was prepared by dissolving 0.14 g sodium in 12.5 mL EtOH, was heated to reflux for 18 h. After cooling to room temperature, the solvent was removed by reduced pressure. EtOAc (75 mL) was added and the precipitate was filtered. The organic layer was washed with water and brine, dried over Na_2SO_4, and evaporated with a rotary evaporator. The crude product was purified by flash chromatography 10:90 EtOAc/CH_2Cl_2 to afford two compounds: ethyl 1-(2-bromophenyl)-4-cyano-5-(4-methoxyphenyl)-*1H*-pyrazole-3-carboxylate **12e**[31] with yield 19% (first major peak) and the desired product **12e′** with yield 12% (second major peak). ^{1}H NMR ($CDCl_3$, δ) 0.95 (t, J =6.8 Hz, 3H, CH_3), 3.85 (s, 3H, OCH_3), 3.92 (q, J = 6.8 Hz, 2H, CH_2), 5.65 (b, NH_2CO), 6.92 (d, J = 8.8 Hz, 2H, ArH), 7.38 (m, 1H, ArH), 7.44–7.52 (m, 2H, ArH), 7.68 (d, J = 8.8 Hz, 2H, ArH), 7.73 (dd, J_1 = 8.0 Hz, J_2 = 1.2 Hz, 1H, ArH). FAB-HRMS: calcd. for $C_{20}H_{19}BrN_3O_4$: 443.0481; found: 444.0538.

4.10. 1-(2-Chloro-4-fluorophenyl)-4-cyano-5-(4-methoxyphenyl)-1*H*-pyrazole-3-carboxylic acid (13a)

A mixture of ethyl 1-(2-chloro-4-fluorophenyl)-4-cyano-5-(4-methoxyphenyl)-1*H*-pyrazole-3-carboxylate **12a** (0.155 g, 0.39 mmol) in 10 mL THF and LiOH (12 mg, 0.49 mmol) in 1 mL water was heated overnight at 65 °C. The reaction mixture was cooled to room temperature, water (25 mL) and 5% HCl (2.5 mL) were added and the mixture was extracted with EtOAc (3×20 mL). The organic layer was washed with brine and dried over Na_2SO_4. The solvent was removed to afford the desired product **13a** with yield 137 mg (95 %). ^{1}H NMR ($CDCl_3$, δ) 3.81 (s, 3H, CH_3), 6.89 (d, J = 6.8 Hz, 2H, ArH), 7.11 (m, 1H, ArH), 7.19 (m, 1H, ArH), 7.26 (d, J = 6.8 Hz, 2H, ArH), 7.49 (m, 1H, ArH). FAB-HRMS: calcd. for $C_{18}H_{11}ClFN_3O_3$: 371.0473; found: 372.0549 $(M+H)^+$.

4.11. 1-(2-Bromo-4-fluorophenyl)-4-cyano-5-(4-methoxyphenyl)-1H-pyrazole-3-carboxylic acid (13b)

Compound **13b** was prepared from ethyl 1-(2-bromo-4-fluorophenyl)-4-cyano-5-(4-methoxyphenyl)-1*H*-pyrazole-3-carboxylate **12b** with the same procedure described for **13a**. Yield was 98 %. ^{1}H NMR ($CDCl_3$, δ) 3.81 (s, 3H, CH_3), 6.88 (d, J = 8.8 Hz, 2H, ArH), 7.16 (m, 1H, ArH), 7.27 (d, J = 8.8 Hz, 2H, ArH), 7.36 (dd, J_1 = 7.6 Hz, J_2 = 2.8 Hz, 2H, ArH),

7.48 (dd, J_1 = 8.8 Hz, J_2 = 5.2 Hz, 2H, ArH). FAB-HRMS: calcd. for $C_{20}H_{11}BrIFN_3O_3$: 414.9968; found: 416.0048 $(M+H)^+$.

4.12. 1-(2,4-Dichlorophenyl)-4-cyano-5-(4-iodophenyl)-1*H*-pyrazole-3-carboxylic acid (13c)

Compound **13c** was prepared from ethyl 1-(2,4-dichlorophenyl)-4-cyano-5-(4-iodophenyl)-1*H*-pyrazole-3-carboxylate **12c** with the same procedure described for **13a** Yield was 99 %. ^{1}H NMR ($CDCl_3$, δ) 7.05 (d, *J* = 8.8 Hz, 2H, ArH), 7.42 (m, 2H, ArH), 7.49 (d, *J* = 2.0 Hz, 1H, ArH), 7.76 (d, *J* = 8.4 Hz, 2H, ArH). FAB-HRMS: calcd. for $C_{17}H_8Cl_2IN_3O_2$: 482.9038; found: 483.9122 $(M+H)^+$.

4.13. 1-(2,4-Dichlorophenyl)-4-cyano-5-(4-bromophenyl)-1*H*-pyrazole-3-carboxylic acid (13d)

Compound **13d** was prepared from ethyl 1-(2,4-dichlorophenyl)-4-cyano-5-(4-bromophenyl)-1*H*-pyrazole-3-carboxylate **12d** with the same procedure described for **13a.** Yield was 99 %. ^{1}H NMR ($CDCl_3$, δ) 7.20 (d, *J* = 8.4 Hz, 2H, ArH), 7.42 (m, 2H, ArH), 7.49 (d, *J* = 2.0 Hz, 1H, ArH), 7.55 (d, *J* = 8.4 Hz, 2H, ArH). FAB-HRMS: calcd. for $C_{17}H_8BrCl_2N_3O_2$: 434.9177; found: 435.9245 $(M+H)^+$.

4.14 1-(2-Chloro-4-fluorophenyl)-4-carbamoyl-5-(4-methoxyphenyl)-1*H*-pyrazole-3-carboxylic acid (13e)

Compound **13e** was prepared from ethyl 1-(2-bromophenyl)-4-carbamoyl-5-(4-methoxyphenyl)-1H-pyrazole-3-carboxylate **12e′** with the same procedure described for **13a**. Yield was 95 %. ^{1}H NMR ($CDCl_3$, δ) 3.84 (s, 3H, CH_3), 5.04 (b, NH_2CO), 6.95 (d, *J* = 8.8 Hz, 2H, ArH), 7.40 (m, 1H, ArH), 7.49 (m, 2H, ArH), 7.71 (d, *J* = 8.8 Hz, 2H, ArH). FAB-HRMS: calcd. for $C_{18}H_{14}BrN_3O_4$: 415.0168; found: 416.0265 $(M+H)^+$.

4.15. 1-(2-Chloro-4-fluorophenyl)-4-cyano-5-(4-methoxyphenyl)-*N*-(piperidin-1-yl)-1*H*-pyrazole-3-carboxamide (7a)

Compound **13a** (0.13 g, 0.35 mmol) was added to a solution containing 1-aminopiperidine (0.07 mL, 0.63 mmol) and triethylamine (0.18 mL) in dichloromethane (10 mL). Then BOP (0.28 g, 0.62 mmol) was added. The mixture was stirred at room temperature for 20 h. The reaction mixture was quenched with 10 mL of cold water and the organic phase was washed with 2% HCl (7 mL); 5% sodium carbonate and brine and dried over anhydrous Na_2SO_4. The solvent was removed and the residue was purified by flash chromatography ($EtOAc/CH_2Cl_2$ 1:1). The final product was obtained with yield 46 mg (29%). ^{1}H NMR ($CDCl_3$, δ) 1.44 (b, 2H, CH_2-py), 1.76 (m, 4H, CH_2-py), 2.91 (b, 4H, CH_2-py), 3.81 (s, 3H, CH_3), 6.87 (d, *J* = 8.8 Hz, 2H, ArH), 7.13 (m, 1H, ArH), 7.21–7.25 (m, 3H, ArH), 7.45 (m, 1H, ArH), 7.56 (b, 1H, NH). FAB-HRMS: calcd. for $C_{23}H_{21}ClFN_5O_2$: 453.1368; found: 454.1423 $(M+H)^+$.

4.16. 1-(2-Bromo-4-fluorophenyl)-4-cyano-5-(4-methoxyphenyl)-N-(piperidin-1-yl)-1*H*-pyrazole-3-carboxamide (7b)

Compound **7b** was prepared from 1-(2-bromo-4-fluorophenyl)-4-cyano-5-(4-methoxyphenyl)-1*H*-pyrazole-3-carboxylic acid **13b** with the same procedure described for **7a**. Yield was 32 %. ^{1}H NMR ($CDCl_3$, δ) 1.43 (b, 2H, CH_2-py), 1.75 (m, 4H, CH_2-py), 2.89 (b, 4H, CH_2-py), 3.80 (s, 3H, CH_3), 6.87 (d, *J* = 8.8 Hz, 2H, ArH), 7.25 (d, *J* = 8.8 Hz, 2H, ArH), 7.39–7.47 (m, 2H, ArH), 7.57 (b, 1H, NH). FAB-HRMS: calcd. for $C_{23}H_{21}BrFN_5O_2$: 497.0863; found: 498.0921 $(M+H)^+$.

4.17. 1-(2,4-dichlorophenyl)-4-cyano-5-(4-iodophenyl)-N-(piperidin-1-yl)-1*H*-pyrazole-3-carboxamide (7c)

Compound **7c** was prepared from 1-(2,4-dichlorophenyl)-4-cyano-5-(4-iodophenyl)-1*H*-pyrazole-3-carboxylic acid **13c** with the same procedure described for **7a**. Yield was 32 %. ^{1}H NMR ($CDCl_3$, δ) 1.44 (b, 2H, CH_2-py), 1.75 (m, 4H, CH_2-py), 2.91 (b, 4H, CH_2-py), 7.04 (d, *J* = 8.8 Hz, 2H, ArH), 7.42 (dd, J_1=8.4 Hz, J_2=2.0 Hz, 1H, ArH), 7.47–7.95 (m, 2H, ArH), 7.57 (b, 1H, NH), 7.73 (d, *J* = 8.8 Hz, 2H, ArH). FAB-HRMS: calcd. for $C_{22}H_{18}Cl_2IN_5O$: 564.9933; found: 565.9987 $(M+H)^+$.

4.18. 1-(2,4-dichlorophenyl)-4-cyano-5-(4-bromophenyl)-N-(piperidin-1-yl)-1*H*-pyrazole-3-carboxamide (7d)

Compound **7d** was prepared from 1-(2,4-dichlorophenyl)-4-cyano-5-(4-bromophenyl)-1*H*-pyrazole-3-carboxylic acid **13d** with the same procedure described for **7a**. Yield was 17 %. ^{1}H NMR ($CDCl_3$, δ) 1.44 (b, 2H, CH_2-py), 1.75 (m, 4H, CH_2-py), 2.89 (b, 4H, CH_2-py), 7.18 (d, *J* = 9.6 Hz, 2H, ArH), 7.42–7.43 (m, 2H, ArH), 7.50 (d, *J* = 1.2 Hz, 1H, ArH), 7.53 (d, *J* = 8.8 Hz, 2H, ArH), 7.55 (b, 1H, NH). FAB-HRMS: calcd. for $C_{22}H_{18}BrCl_2N_5O$: 517.0072; found: 518.0172 $(M+H)^+$.

4.19. 1-(2-bromophenyl)-5-(4-methoxyphenyl)-N^3-(piperidin-1-yl)-1H-pyrazole-3,4-dicarboxamide (7e)

Compound **7e** was prepared from 1-(2-chloro-4-fluorophenyl)-4-cyano-5-(4-methoxyphenyl)-1*H*-pyrazole-3-carboxylic acid **13e** with the same procedure described for **7a**. Yield was 22 %. ^{1}H NMR ($CDCl_3$, δ) 1.36 (b, 2H, CH_2-py), 1.64 (m, 4H, CH_2-py), 2.69 (b, 4H, CH_2-py), 3.85 (s, 3H, CH_3), 5.45 (b, 2H, NH_2CO), 6.88 (d, *J* = 8.8 Hz, 2H, ArH), 7.43 (m, 1H, ArH), 7.50 (m, 2H, ArH), 7.71 (d, *J* = 8.8 Hz, 2H, ArH), 7.77 (b, 1H, NH). FAB-HRMS: calcd. for $C_{23}H_{24}BrN_5O_3$: 497.1063; found: 498.1141 $(M+H)^+$.

4.20. 1-(2,4-dichlorophenyl)-4-cyano-5-(4-iodophenyl)-*N*-morpholino-1*H*-pyrazole-3-carboxamide (7f)

Compound **7f** was prepared from 1-(2,4-dichlorophenyl)-4-cyano-5-(4-iodophenyl)-1*H*-pyrazole-3-carboxylic acid **13c** and *N*-aminomorpholine with the same procedure described for **7a**. Yield was 35 %. ^{1}H NMR ($CDCl_3$, δ) 2.98 (t, *J* =4.4 Hz, 4H, CH_2-py), 3.86 (t, *J* =4.4 Hz, 4H, CH_2-py), 7.03 (d, *J*=8.0 Hz, 2H, ArH), 7.42 (m, 2H, ArH), 7.51 (m, 1H, ArH), 7.60 (b, 1H, NH) 7.74 (d, *J*=8.0 Hz, 2H, ArH). FAB-HRMS: calcd. for $C_{21}H_{16}Cl_2IN_5O_2$: 566.9726; found: 567.9792 $(M+H)^+$.

4.21 1-(2,4-dichlorophenyl)-4-cyano-5-(4-bromophenyl)-*N*-morpholino-1*H*-pyrazole-3-carboxamide (7g)

Compound **7g** was prepared from 1-(2,4-dichlorophenyl)-4-cyano-5-(4-bromophenyl)-1*H*-pyrazole-3-carboxylic acid **13d** and *N*-aminomorpholine with the same procedure described for **7a**. Yield was 35%. ^{1}H NMR ($CDCl_3$, δ) 2.98 (t, *J* =4.8 Hz, 4H, CH_2-py), 3.85 (t, *J* =4.8 Hz, 4H, CH_2-py), 7.18 (d, *J*=8.4 Hz, 2H, ArH), 7.44 (m, 2H, ArH), 7.50 (m, 1H, ArH), 7.53 (d, *J*=8.8 Hz, 2H, ArH), 7.62 (b, 1H, NH) FAB-HRMS: calcd. for $C_{21}H_{16}BrCl_2N_5O_2$: 518.9864; found: 519.9921 $(M+H)^+$.

4.22. 1-(2,4-dichlorophenyl)-4-cyano-5-(4-methoxyphenyl)-N-(pyrrolidin-1-yl)-1*H*-pyrazole-3-carboxamide (7h)

Compound **7h** was prepared from 1-(2,4-dichlorophenyl)-4-cyano-5-(4-methoxyphenyl)-1*H*-pyrazole-3-carboxylic acid **13f** [31] and 1-aminopyrrolidine hydrochloride with the same procedure described for **7a**. Yield was 15 %. ^{1}H NMR ($CDCl_3$, δ) 1.91 (m, 4H, CH_2-py), 3.05

(b, 4H, CH_2-py), 3.81 (s, 3H, CH_3), 6.88 (d, *J* = 8.4 Hz, 2H, ArH), 7.23 (d, *J* = 8.4 Hz, 2H, ArH), 7.37–7.39 (m, 2H, ArH), 7.49 (d, *J* = 1.6 Hz, 1H, ArH), 7.54 (b, 1H, NH). FAB-HRMS: calcd. for $C_{22}H_{19}Cl_2N_5O_2$: 455.0916; found: 456.0977 $(M+H)^+$.

4.23. 1-(2,4-dichlorophenyl)-4-cyano-5-(4-(fluoromethoxy)phenyl)-*N*-(piperidin-1-yl)-1*H*-pyrazole-3-carboxamide (7i)

Fluoromethyltosylate [38] (41 mg, 0.24 mmol) was added to a solution of 1-(2,4-dichlorophenyl)-4-cyano-5-(4-hydroxyphenyl)-*N*-(piperidin-1-yl)-1*H*-pyrazole-3-carboxamide[31] (91 mg, 0.2 mmol) and potassium carbonate (55 mg, 0.4 mmol) in acetone (10 mL) and the mixture was refluxed for 2 days. The reaction mixture was cooled and solvent was removed. The residue was diluted with saturated ammonium chloride solution, extracted with ethyl acetate and washed with water. The organic layer was dried over Na_2SO_4 and solvent was removed at reduced pressure. The residue was separated by flash chromatography (hexanes/EtOAc (3:1)). Yield was 35 mg (36%). ^{1}H NMR ($CDCl_3$, δ) 1.44 (b, 2H, CH_2-py), 1.75 (m, 4H, CH_2-py), 2.90 (b, 4H, CH_2-py), 5.67 (d, *J* = 54.4 Hz, 2H, OCH_2F), 7.07 (d, *J* = 8.4 Hz, 2H, ArH), 7.29 (d, *J* = 8.8 Hz, 2H, ArH), 7.40 (d, *J* = 1.6 Hz, 2H, ArH), 7.48 (t, *J* = 1.6 Hz, 1H, ArH), 7.54 (b, 1H, NH). FAB-HRMS: calcd. for $C_{23}H_{20}Cl_2FN_5O_2$: 487.0978; found: 488.1068 $(M+H)^+$

4.24. 1-(2,4-dichlorophenyl)-4-cyano-5-(4-hydroxyphenyl)-*N*-(pyrrolidin-1-yl)-1*H*-pyrazole-3-carboxamide (16)

5-(4-(allyloxy)phenyl)-1-(2,4-dichlorophenyl)-4-cyano-*N*-(pyrrolidin-1-yl)-1*H*-pyrazole-3-carboxamide **18** was prepared from 5-(4-(allyloxy)phenyl)-1-(2,4-dichlorophenyl)-4-cyano-1*H*-pyrazole-3-carboxylic acid **17**[31] and 1-aminopyrrolidine hydrochloride with the same procedure described for **7a**. Yield of **18** was 72 %. A mixture of **18** (172 mg, 0.36 mmol), $Pd(PPh_3)_4$ (8.2 mg, 7.1 μmol), and $PhSiH_3$ (78 mg, 0.72 mmol) in 150 mL CH_2Cl_2 was stirred at room temperature for 1 h. Then the solvent was removed and EtOAc (20 mL) was added to the residue. The organic layer was washed with saturated $NaHCO_3$, brine, and dried over Na_2SO_4. The crude product was purified by flush chromatography, EtOAc/CH_2Cl_2 (1:1), The final product **16** was obtained with yield 95 mg (60%). ^{1}H NMR ($CDCl_3$, δ) 1.91 (m, 4H, CH_2-py), 3.05 (b, 4H, CH_2-py), 6.87 (dd, J_1 = 6.4 Hz, J_2 = 1.6 Hz, 2H), 7.19 (dd, J_1 = 6.2 Hz, J_2 = 1.5 Hz, 2H), 7.40 (m, 2H), 7.54 (d, *J* = 2.0 Hz, 1H), 7.64 (b, 1H). FAB-HRMS: calcd. for $C_{21}H_{17}Cl_2N_5O_2$: 441.0759; found: 442.0838 $(M+H)^+$.

4.25. In vitro inhibition binding assay

The *in vitro* inhibition binding assays of all CB1 ligands (Table 1) were performed commercially by NovaScreen (Hanover, MD) under the experimental conditions similar to those previously published.[31,48] Briefly, membranes from HEK-293 cells expressing the human recombinant cannabinoid receptor CB1 were incubated with [^{3}H]CP55,940 (K_d=0.6 nM) at a concentration of 0.5 nM in 50 mM Tris-HCl buffer with 5 mM $MgCl_2$, 5 mg/ml BSA and 2.5 mM EDTA at pH 7.4 for 90 minutes at 30°C. The binding reaction was terminated by rapid vacuum filtration of the assay contents onto presoaked (0.5% PEI) Whatman GF/C filters. Radioactivity trapped onto the filters was assessed using liquid scintillation counting. Non-specific binding was defined as that remaining in the presence of 1 μM HU-210. The assays were done in duplicate at multiple concentrations of the test compounds. Binding assay results were analyzed using a one site competition models and IC_{50} curves were generated based on a sigmoidal dose response with variable slope. Values of K_i were calculated using Cheng-Prusoff equation.[49]

4.26. Functional assay

Coronal brain slices (250–300 μm) containing the striatum were prepared from 2–4 month old C57/BL6 mice based on previously published protocols.[50,51] Extracellular recordings were performed using a differential AC amplifier (A-M Systems, Model 1700) and electrodes pulled from thick-walled borosilicate capillary tubing (0.75 mm ID, 1.5 mm OD, Sutter Instruments, Novato, CA) filled with 3M NaCl solution. During the recording, slices were maintained at 32–33 °C and were continuously superfused at a rate of 2 ml/min with a modified artificial cerebrospinal fluid (aCSF) consisting of (in mM) NaCl, 126; KCl, 3.0; $MgCl_2$, 1.5; $CaCl_2$, 2.4; NaH_2PO_4, 1.2; glucose, 11.0; $NaHCO_3$, 26, and saturated with 95% O_2 and 5% CO_2. In order to isolate glutamate-driven synaptic potentials[52] the aCSF also contained the $GABA_A$-receptor antagonist picrotoxin (100 μM) and the N-methyl-D-Aspartate (NMDA)-type receptor antagonist APV (40 μM). Electrical stimulation was performed using a bipolar tungsten stimulating electrode placed near (< 100 μm) the recording electrode, in the dorsal striatum. Single, 0.1 ms pulses (10–30 V) were delivered to the stimulating electrode at a frequency of 0.033 Hz. Following establishment of a stable baseline response (≥ 10 min), drugs were applied *via* bath superfusion. Data were acquired and stored on a Pentium-based PC computer via an A/D board (National Instruments PCI 6024E, Austin, TX), using a Windows-based software package (courtesy of Dr. John Dempster, University of Strathclyde, Glasgow, UK). Analyses of peak synaptic potential amplitudes were performed off-line using the same software. Responses were normalized by averaging the control (baseline, pre-drug) responses, and post-drug effects were determined by averaging 5–10 sweeps during the peak of the response. A paired, two-tailed t-test (GraphPad Prism v 5.0, GraphPad Scientific, San Diego CA) was then performed between the pre-drug and post-drug responses in order to determine statistical significance at an α value of 0.05 (e.g., $p \leq 0.05$ was considered statistically significant).

4.27. Molecular Modeling

Conformational Analysis—Complete conformational analyses of **4** and **7e** were performed using *ab initio* Hartree-Fock calculations at the 3-21G* level, within the Spartan molecular modeling program (Wavefunction, Inc., Irvine, CA). HF 3-21G* 6-fold conformer searches were performed for the rotateable bonds (C3 substituent: C3-C1′ and N2′-N3′; C5 substituent: C5-C1‴; N1 substituent: N1-C1″). In each conformer search, local energy minima were identified by rotation of a subject torsion angle through 360° in 60° increments (6-fold search), followed by HF 3-21G* energy minimization of each rotamer generated.

In order to compare the energy of the conformers of **4** to that of **1**,[43] an *ab initio* geometry optimization at the HF 6-31G* level was performed for the global minimum energy conformer of **4** identified by the HF 3-21G* conformational search and for the second to global minimum energy conformer of **4**. The energy separation between conformers reported in the text was calculated using results from these *ab initio* HF calculations at the 6-31G* level as encoded in Jaguar (version 6.0, Schrodinger, LLC, New York, NY). To calculate the energy difference between the global minimum energy conformer of the compound and its final docked conformation, rotateable bonds in the global minimum energy conformer were driven to their corresponding value in the final docked conformation and the single point energy of the resultant structure was calculated at the HF 6-31G* level.

Ligand-Receptor Complex Modeling

Ligand Docking and Energy Minimization of Ligand/CB1 R Complex—Receptor residues are numbered here using the amino acid numbering scheme proposed by Ballesteros and Weinstein.[53] Compound **4** was docked using interactive computer graphics in a recently described TMH model of the CB1 receptor inactive state (R).[43] The ligand was docked within the aromatic residue rich TMH3-4-5-6 region of the bundle in the same orientation as its

structural analog **1**. The complex was then energy minimized using the Amber* united atom force field in Macromodel (version 8.6, Schrödinger, LLC, New York, NY) and our previously published protocol.[43] Interactive docking methods were used here because the binding region in CB1 for **1** (TMH3-4-5-6) and the nature of specific ligand functional group/specific amino acid interactions are known from mutation/chimera studies. The combined information limits the ligand to one particular region of CB1 and to one particular orientation in this region. Given the following experimental evidence, we consider the approach here to be appropriate: Shire and co-workers have shown in CB1/CB2 chimera studies that the TMH4-EC2-TMH5 region of CB1 contains residues critical for the binding of **1**.[54] Subsequent CB1 F3.36(200)A, W5.43(279)A, and W6.48(356)A mutation studies published by our group indicated that the binding of **1** is affected by each of these mutations, suggesting that these residues are part of the binding site for **1**.[41] Our previous mutant cycle study indicated that K3.28(192) is involved in a direct interaction with the C3 substituent of **1** in wild-type (WT) CB1.[42] Recent analog synthesis/CB1 binding results suggest that this direct interaction is between K3.28(192) and the carboxamide oxygen of **1**.[43] This result fixes the orientation of **1** in the CB1 bundle to be that pictured in Figure 5B.

The energy of each ligand/CB1 R TMH bundle complex was minimized using the AMBER* united atom force field in Macromodel (version 8.6, Schrödinger, LLC, New York, NY). A distance dependent dielectric, 8.0 Å extended nonbonded cutoff (updated every 10 steps), 20.0 Å electrostatic cutoff, and 4.0 Å hydrogen bond cutoff were used. During the minimization a 10,000 kcal/mol force was used to restrain the rotation of the N1 substituent dichlorophenyl, the C5 substituent para-methoxyphenyl and the piperidine rings. The first stage of the calculation consisted of 2000 steps of Polak-Ribier conjugate gradient (CG) minimization in which a force constant of 225 kJ/mol was used on the helix backbone atoms in order to hold the TMH backbones fixed, while permitting the side chains to relax. The second stage of the calculation consisted of 100 steps of CG in which the force constant on the helix backbone atoms was reduced to 50 kJ/mol in order to allow the helix backbones to adjust. Stages one and two were repeated with the number of CG steps in stage two incremented from 100 to 500 steps until a gradient of 0.04 kJ/(mol Å ^{2}) was reached.

Assessment of Aromatic Stacking Interactions—Aromatic-aromatic (π–π) stacking interactions were identified in the minimized ligand/receptor complexes based upon criteria defined by Burley and Petsko for the ring centroid to centroid distance (d) and the angle between normal vectors of interacting aromatic rings (α).[55] These interactions were further classified as tilted-T arrangements if $30° < \theta < 90°$ and as parallel arrangements for $\theta < 30°$. Parallel arrangements were considered favorable only if the interacting rings were offset from each other.[56] All measurements were made using Maestro (version 7.0, Schrodinger, LLC, New York, NY).

Assessment of Pair-wise Interaction Energies—After defining the atoms of each ligand as one group (Group 1) and the atoms corresponding to a residue that lines the binding site in the final ligand/CB1 R complex as another group (Group 2), Macromodel (version 8.6, Schrödinger, LLC, New York, NY) was used to output the pair interaction energy (coulombic and van der Waals) for a given pair of atoms. The pairs corresponding to Group 1 (ligand) and Group 2 (residue of interest) were then summed to yield the interaction energy between the ligand and that residue.

4.28. Radiochemistry

1-(2,4-dichlorophenyl)-4-cyano-[^{11}C]5-(4-methoxyphenyl)-N-(pyrrolidin-1-yl)-1H-pyrazole-3- carboxamide ([^{11}C]7h)—Precursor, 1-(2,4-dichlorophenyl)-4-cyano-5-(4-hydroxyphenyl)-N-(pyrrolidin-1-yl)-1*H*-pyrazole-3-carboxamide **16,** (1 mg) was

added to a 1 mL reaction vial. The precursor was dissolved in 0.2 mL of acetone. Five microliters of 2 M sodium hydroxide was added, and the vial was capped with a septum seal and shaken. No-carrier-added ^{11}C-labeled methyl triflate prepared as described previously [57] was swept by nitrogen flow into the vial. The reaction mixture was heated for 3 min at 45 °C and diluted with 200 μL of water. The mixture was injected into a Phenomenex Luna C18 column (10 × 250 mm) and eluted with CH_3CN : 0.1M aqueous ammonium formate buffer 60:40 at a flow rate of 10 mL/min. The radioactive peak of [^{11}C]**7h** with retention time 7–8 min was collected into a flask and the solvent was removed on a rotary-evaporator. The product was reconstituted in ethanol (1 mL) and sterile 0.9% saline (9.0 mL) and passed through a 0.2 μM sterile filter (Millex-FG, Millipore) into a sterile, pyrogen-free multi-dose vial. The non-decay corrected radiochemical yield for [^{11}C]**7h** was 15–24%.

An aliquot of the final solution of known volume and radioactivity was applied to an analytical reverse-phase HPLC column (Luna C18 column, 250 mm × 4.6 mm; a mobile phase of CH_3CN : 0.1M aqueous ammonium formate buffer 60:40; flow rate of 5 mL/min). The desired product was eluted with a retention time of 2.5 min. The area of the UV absorbance peak at 254 nm corresponding to product was measured and compared to a standard curve relating mass to UV absorbance. The average specific radioactivity of the final product ([^{11}C]**7h**) was 482±288 GBq/μmol (13019±7800 mCi/μmol) (n=5). The radiochemical product was co-eluted with a standard of "cold" **7h**.

4.29. Mice studies

Baseline Study—Male, CD-1 mice weighing 25–30 g from Charles River Laboratories, (Wilmington, MA) were used for biodistribution studies. The animals were sacrificed by cervical dislocation at various times (3 animals per time-point) following injection of [^{11}C]**7h** or [^{11}C]**15** (~7.4 MBq; ~200 μCi), specific radioactivity was about 200–240 GBq/μmol (5,400 - 6,400 mCi/μmol) in 0.2 mL saline) into a lateral tail vein. The brains were rapidly removed and dissected on ice. The brain regions of interest were weighed and their radioactivity content was determined in an automated γ-counter with a counting error below 3%. Aliquots of the injectate were prepared as standards and their radioactivity content was counted along with the tissue samples. The percent of injected dose per gram of tissue (%ID/g tissue) was calculated. All experimental protocols were approved by the Animal Care and Use Committee of the Johns Hopkins Medical Institutions.

Blocking with Rimonabant 1—*In vivo* CB1 receptor blocking studies were performed by intravenous (i.v.) administration of 1 mg/kg of Rimonabant **1** followed by i.v. injection in three animals of [^{11}C]**7h** (~7.4 MBq; ~200 μCi) with specific radioactivity ~300 GBq/μmol (8,100 mCi/μmol) 15 min thereafter. Rimonabant **1** was dissolved in a vehicle solution (saline:alcohol:Cremophore-EL (9:1:0.06)) and administered in a volume of 0.1 mL. Control animals (three animals) were injected with 0.1 mL of the vehicle solution. Sixty min after administration of the tracer the brain tissues were harvested and their radioactivity content was determined.

The animal statistical data analysis was performed with Microsoft Excel software with ANOVA single factor analysis tool kit, $p \leq 0.05$ was considered statistically significant.

Acknowledgments

The authors are grateful to Ms. Paige Finley for the rodent experiments and Ms. Judy W. Buchanan for editorial work. This work was supported in part by NIH/NIMH grant MH-079017 (AGH) and NIH/NIDA Grants DA-03934 and DA-021358 (PHR).

References

1. Howlett AC, Barth F, Bonner TI, Cabral G, Casellas P, Devane WA, Felder CC, Herkenham M, Mackie K, Martin BR, Mechoulam R, Pertwee RG. Pharmacol Rev 2002;54:161–202. [PubMed: 12037135]
2. Gong JP, Onaivi ES, Ishiguro H, Liu QR, Tagliaferro PA, Brusco A, Uhl GR. Brain Res 2006;1071:10–23. [PubMed: 16472786]
3. Pertwee RG. International Journal of Obesity 2006;30:S13–S18. [PubMed: 16570099]
4. Rinaldi-Carmona M, Barth F, Heaulme M, Shire D, Calandra B, Congy C, Martinez S, Maruani J, Neliat G, Caput D, et al. FEBS Lett 1994;350:240–244. [PubMed: 8070571]
5. Van Gaal LF, Rissanen AM, Scheen AJ, Ziegler O, Rossner S. Lancet 2005;365:1389–1397. [PubMed: 15836887]
6. Cleland JG, Ghosh J, Freemantle N, Kaye GC, Nasir M, Clark AL, Coletta AP. Eur J Heart Fail 2004;6:501–508. [PubMed: 15182777]
7. Cota D, Marsicano G, Lutz B, Vicennati V, Stalla GK, Pasquali R, Pagotto U. Int J Obes Relat Metab Disord 2003;27:289–301. [PubMed: 12629555]
8. Vickers SP, Kennett GA. Curr Drug Targets 2005;6:215–223. [PubMed: 15777191]
9. Witkin JM, Tzavara ET, Nomikos GG. Behav Pharmacol 2005;16:315–331. [PubMed: 16148437]
10. Witkin JM, Tzavara ET, Davis RJ, Li X, Nomikos GG. Trends Pharmacol Sci 2005;26:609–617. [PubMed: 16260047]
11. Hungund BL, Vinod KY, Kassir SA, Basavarajappa BS, Yalamanchili R, Cooper TB, Mann JJ, Arango V. Mol Psychiatry 2004;9:184–190. [PubMed: 14966476]
12. Vinod KY, Arango V, Xie S, Kassir SA, Mann JJ, Cooper TB, Hungund BL. Biol Psychiatry 2005;57:480–486. [PubMed: 15737662]
13. Schlicker E, Kathmann M. Trends Pharmacol Sci 2001;22:565–572. [PubMed: 11698100]
14. Huestis MA, Gorelick DA, Heishman SJ, Preston KL, Nelson RA, Moolchan ET, Frank RA. Arch Gen Psychiatry 2001;58:322–328. [PubMed: 11296091]
15. Le Foll B, Goldberg SR. J Pharmacol Exp Ther 2005;312:875–883. [PubMed: 15525797]
16. De Vries TJ, Schoffelmeer AN. Trends Pharmacol Sci 2005;26:420–426. [PubMed: 15992935]
17. Lange JH, Kruse CG. Drug Discov Today 2005;10:693–702. [PubMed: 15896682]
18. Mathews WB, Ravert HT, Musachio JL, Frank RA, Rinaldi-Carmona M, Barth F, Dannals RF. Journal of Labelled Compounds & Radiopharmaceuticals 1999;42:589–596.
19. Mathews WB, Scheffel U, Finley P, Ravert HT, Frank RA, Rinaldi-Carmona M, Barth F, Dannals RF. Nucl Med Biol 2000;27:757–762. [PubMed: 11150708]
20. Mathews WB, Scheffel U, Rauseo PA, Ravert HT, Frank RA, Ellames GJ, Herbert JM, Barth F, Rinaldi-Carmona M, Dannals RF. Nucl Med Biol 2002;29:671–677. [PubMed: 12234592]
21. Katoch-Rouse R, Pavlova OA, Caulder T, Hoffman AF, Mukhin AG, Horti AG. Journal of Medicinal Chemistry 2003;46:642. [PubMed: 12570386]
22. Willis PG, Katoch-Rouse R, Horti AG. Journal of Labelled Compounds & Radiopharmaceuticals 2003;46:799.
23. Katoch-Rouse R, Horti AG. Journal of Labelled Compounds & Radiopharmaceuticals 2003;46:93.
24. Gatley SJ, Gifford AN, Ding YS, Volkow ND, Lan R, Liu Q, Makriyannis A. Drug Discovery Strategies and Methods 2004:129–146.
25. Gatley SJ, Lan R, Volkow ND, Pappas N, King P, Wong CT, Gifford AN, Pyatt B, Dewey SL, Makriyannis A. J Neurochem 1998;70:417–423. [PubMed: 9422389]
26. Li Z, Gifford A, Liu Q, Thotapally R, Ding YS, Makriyannis A, Gatley SJ. Nucl Med Biol 2005;32:361–366. [PubMed: 15878505]
27. Berding G, Muller-Vahl K, Schneider U, Gielow P, Fitschen J, Stuhrmann M, Harke H, Buchert R, Donnerstag F, Hofmann M, Knoop BO, Brooks DJ, Emrich HM, Knapp WH. Biol Psychiatry 2004;55:904–915. [PubMed: 15110734]
28. Berding G, Schneider U, Gielow P, Buchert R, Donnerstag F, Brandau W, Knapp WH, Emrich HM, Muller-Vahl K. Psychiatry Res. 2006

29. Katoch-Rouse, R.; Chefer, SI.; Pavlova, OA.; Vaupel, DB.; Matochik, JA.; Caulder, T.; Hoffman, A.; Kimes, AS.; Mukhin, AG.; Horti, AG. IX Symposium on the Medical Applications of Cyclotrons; Turku, Finland. 2002.
30. Katoch-Rouse R, Pavlova OA, Caulder T, Hoffman AF, Mukhin AG, Horti AG. J Med Chem 2003;46:642–645. [PubMed: 12570386]
31. Fan H, Ravert HT, Holt D, Dannals RF, Horti AG. Journal of Labelled Compounds and Radiopharmaceuticals 2006;49:1021–1036.
32. Horti AG, Fan H, Kuwabara H, Hilton J, Ravert HT, Holt DP, Alexander M, Kumar A, Rahmim A, Scheffel U, Wong DF, Dannals RF. J Nucl Med 2006;47:1689–1696. [PubMed: 17015906]
33. Yasuno F, Brown AK, Zoghbi SS, Krushinski JH, Chernet E, Tauscher J, Schaus JM, Phebus LA, Chesterfield AK, Felder CC, Gladding RL, Hong J, Halldin C, Pike VW, Innis RB. Neuropsychopharmacology. 2007
34. Burns HD, Van Laere K, Sanabria-Bohorquez S, Hamill TG, Bormans G, Eng WS, Gibson R, Ryan C, Connolly B, Patel S, Krause S, Vanko A, Van Hecken A, Dupont P, De Lepeleire I, Rothenberg P, Stoch SA, Cote J, Hagmann WK, Jewell JP, Lin LS, Liu P, Goulet MT, Gottesdiener K, Wagner JA, de Hoon J, Mortelmans L, Fong TM, Hargreaves RJ. Proc Natl Acad Sci U S A 2007;104:9800–9805. [PubMed: 17535893]
35. F. Barth, S. Martinez, M. Rinaldi-Carmona, (Sanofi-Synthelabo, Fr.). Application: FR FR, 2004, p. 22 pp.
36. L. Emmel, G. Heubach, (Farbwerke Hoechst A.-G.). Application: DE DE, 1971, p. 15 pp.
37. Larsen SD, Spilman CH, Bell FP, Dinh DM, Martinborough E, Wilson GJ. J Med Chem 1991;34:1721–1727. [PubMed: 2033594]
38. Iwata R, Furumoto S, Pascali C, Bogni A, Ishiwata K. Journal of Labelled Compounds & Radiopharmaceuticals 2003;46:555–566.
39. Gonsiorek W, Lunn C, Fan X, Narula S, Lundell D, Hipkin RW. Mol Pharmacol 2000;57:1045–1050. [PubMed: 10779390]
40. Lan R, Liu Q, Fan P, Lin S, Fernando SR, McCallion D, Pertwee R, Makriyannis A. J Med Chem 1999;42:769–776. [PubMed: 10052983]
41. McAllister SD, Rizvi G, Anavi-Goffer S, Hurst DP, Barnett-Norris J, Lynch DL, Reggio PH, Abood ME. J Med Chem 2003;46:5139–5152. [PubMed: 14613317]
42. Hurst DP, Lynch DL, Barnett-Norris J, Hyatt SM, Seltzman HH, Zhong M, Song ZH, Nie J, Lewis D, Reggio PH. Mol Pharmacol 2002;62:1274–1287. [PubMed: 12435794]
43. Hurst D, Umejiego U, Lynch D, Seltzman H, Hyatt S, Roche M, McAllister S, Fleischer D, Kapur A, Abood M, Shi S, Jones J, Lewis D, Reggio P. J Med Chem 2006;49:5969–5987. [PubMed: 17004712]
44. Robbe D, Alonso G, Duchamp F, Bockaert J, Manzoni OJ. Journal of Neuroscience 2001;21:109. [PubMed: 11150326]
45. Ronesi J, Gerdeman GL, Lovinger DM. J Neurosci 2004;24:1673–1679. [PubMed: 14973237]
46. Reggio PH. Curr Pharm Des 2003;9:1607–1633. [PubMed: 12871061]
47. Herkenham M, Lynn AB, Johnson MR, Melvin LS, de Costa BR, Rice KC. J Neurosci 1991;11:563–583. [PubMed: 1992016]
48. Thomas BF, Gilliam AF, Burch DF, Roche MJ, Seltzman HH. J Pharmacol Exp Ther 1998;285:285–292. [PubMed: 9536023]
49. Cheng Y, Prusoff WH. Biochem Pharmacol 1973;22:3099–3108. [PubMed: 4202581]
50. Hoffman AF, Lupica CR. J Neurophysiol 2001;85:72–83. [PubMed: 11152707]
51. Hoffman AF, Macgill AM, Smith D, Oz M, Lupica CR. Eur J Neurosci 2005;22:2387–2391. [PubMed: 16262678]
52. Pennartz CM, Boeijinga PH, Lopes da Silva FH. Brain Res 1990;529:30–41. [PubMed: 1980846]
53. Ballesteros, JA.; Weinstein, H. Methods in Neuroscience. Sealfon, SC., editor. Academic Press; San Diego, CA: 1995. p. 366-428.Chapter 319
54. Shire D, Calandra B, Bouaboula M, Barth F, Rinaldi-Carmona M, Casellas P, Ferrara P. Life Sci 1999;65:627–635. [PubMed: 10462063]
55. Burley SK, Petsko GA. Science 1985;229:23–28. [PubMed: 3892686]

56. Hunter CA, Singh J, Thornton JM. J Mol Biol 1991;218:837–846. [PubMed: 2023252]
57. Jewett DM. Applied Radiation and Isotopes 1992;43:1383–1385. [PubMed: 1333459]

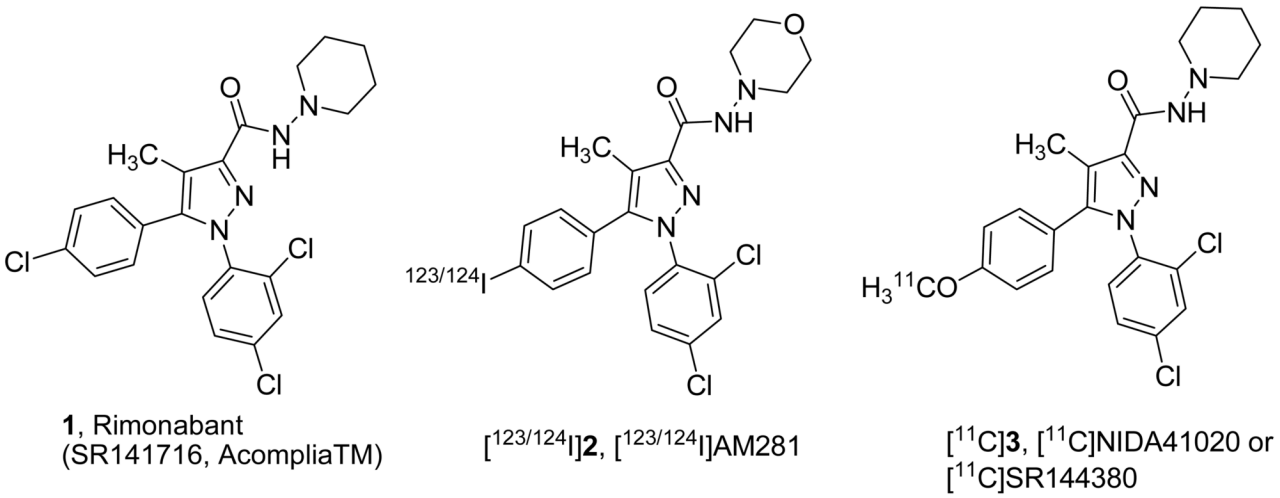

Figure 1.
Representative cannabinoid ligands and radioligands.

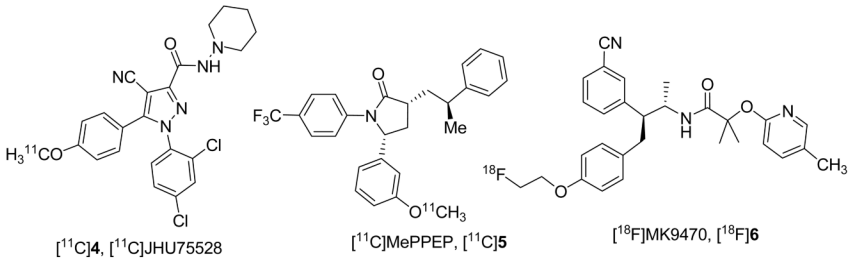

Figure 2.
Latest radioligands for emission tomography imaging of CB1 receptors.

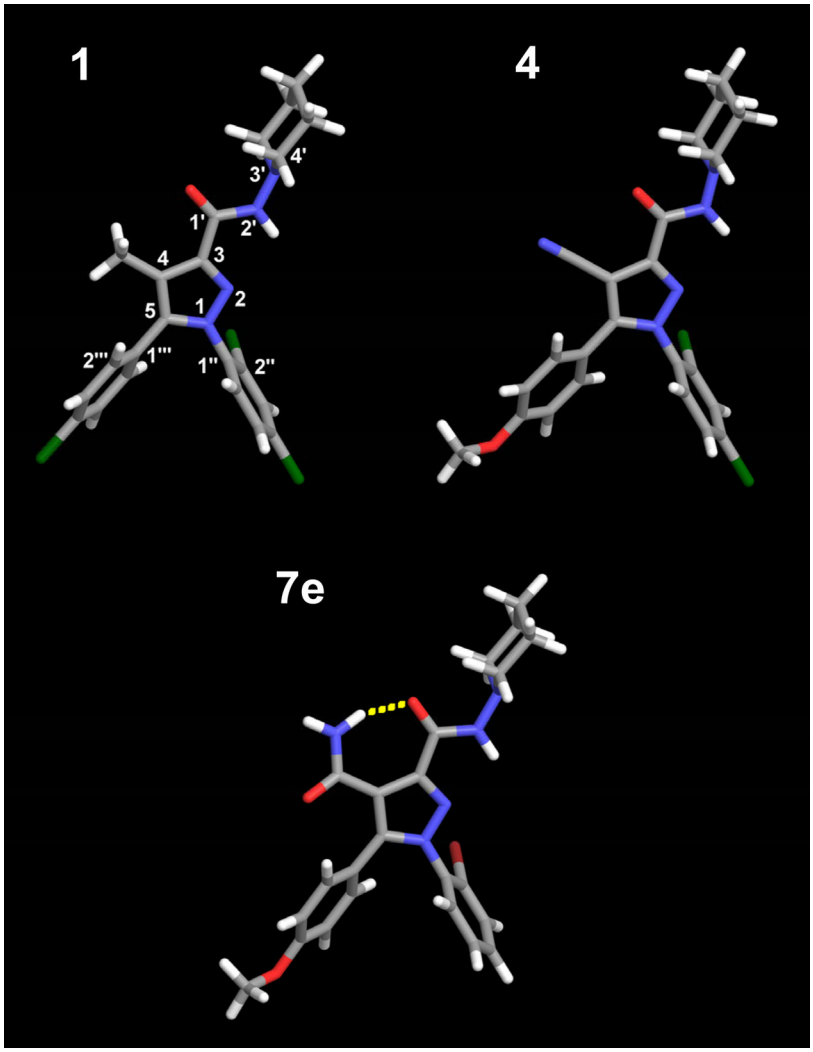

Figure 3.
The global minimum energy conformers of compounds **1**, **4** and **7e** are illustrated here. Compound **7e** was found to have an intramolecular hydrogen bond between the C4 carboxamide nitrogen and the C3 carboxamide oxygen.

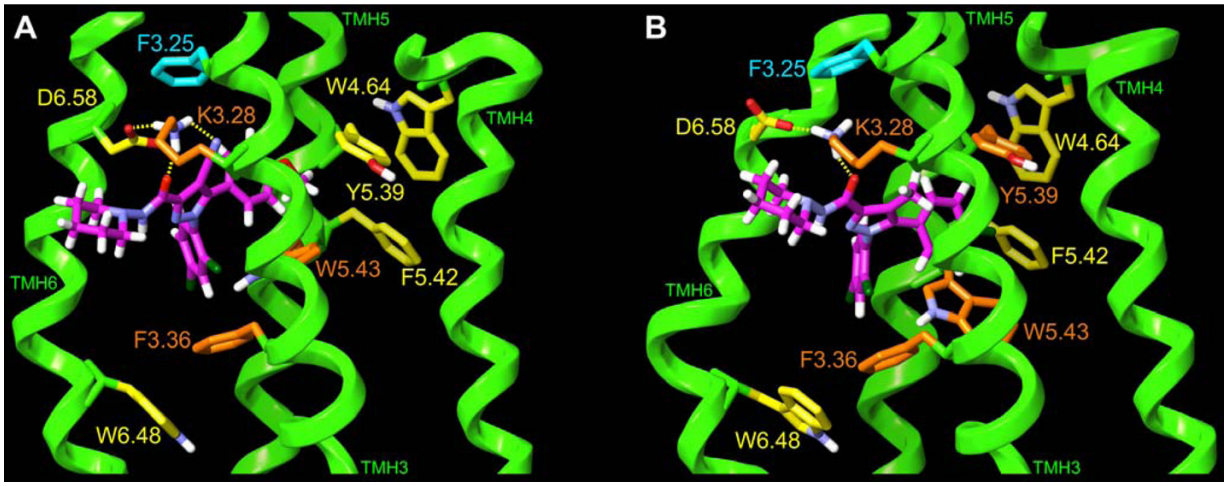

Figure 4.

(**A**) **4** in a minimum energy conformation (ΔE= 1.25 kcal/mol) and (**B**) **1** in a minimum energy conformation (ΔE= 0.92 kcal/mol) are shown here docked in the TMH3-4-5-6 aromatic microdomain within a CB1 TMH bundle model of the R state. The view here is from lipid, looking towards TMHs 3 and 4. TMHs 1, 2 and 7 are not shown in order to simplify the view. Aromatic residues for which each ligand has a direct aromatic stacking interaction are colored orange. Aromatic residues that are part of the extended aromatic cluster, but that do not stack directly with the ligand are colored yellow, while those aromatic residues that have no direct or indirect interaction with the ligand are colored cyan.

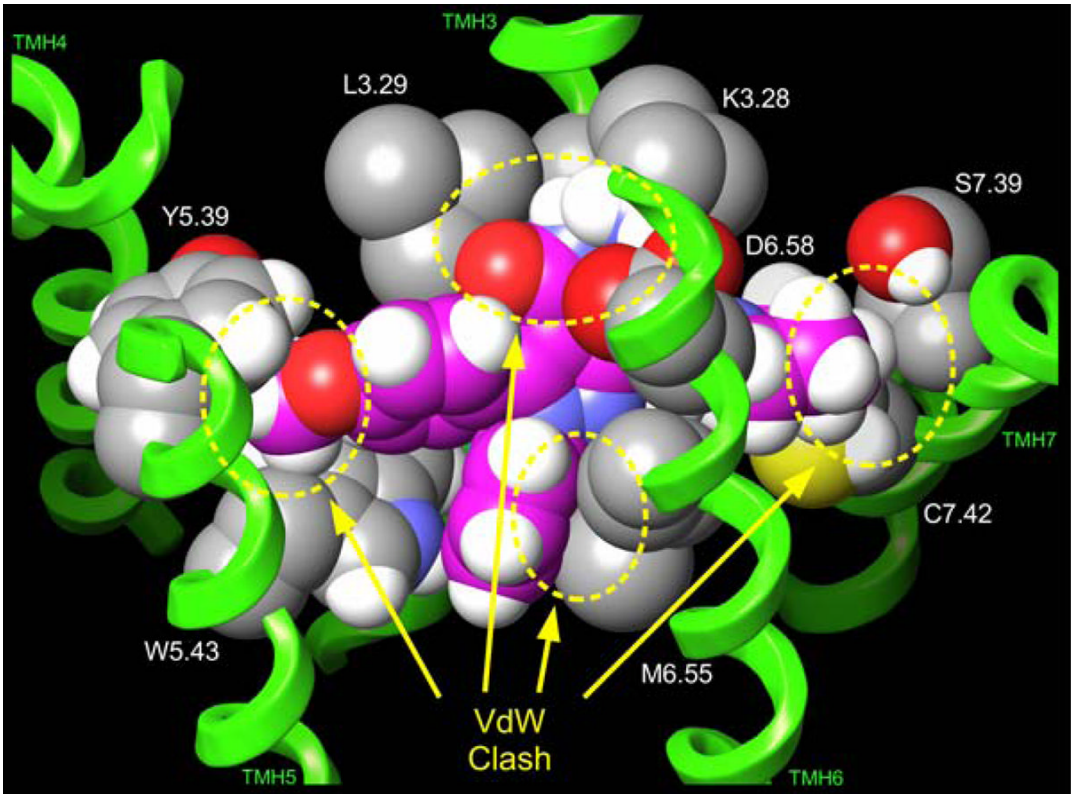

Figure 5.

Compound **7e** has a K_i> 10,000 nM at CB1 (see Table 1). This figure illustrates that compound **7e** exceeds the steric limitations of the CB1 R TMH3-4-5-6 aromatic microdomain binding site in nearly every direction. The most severe steric clash results from the substitution of the amide group for the cyano group in **4**. This produces a severe steric clash between the C4 substituent amide nitrogen of **7e** and residues K3.28(192) and D6.58(366), as well as a clash between the C4 carboxamide oxygen and residue L3.29(193). A severe steric clash also exists between the **7e** piperidine ring and residues C7.42(386) and S7.39(383), as well as between the methoxy group of the C5 substituent para-methoxyphenyl ring and residues Y5.39(275) and W5.43(279). Finally, there is a steric clash between the bromine of the **7e** N1 substituent ortho-bromophenyl ring and residue V3.32(196) (not shown in Figure 4) and the phenyl ring of the **7e** N1 substituent ortho-bromophenyl ring and residue M6.55(363).

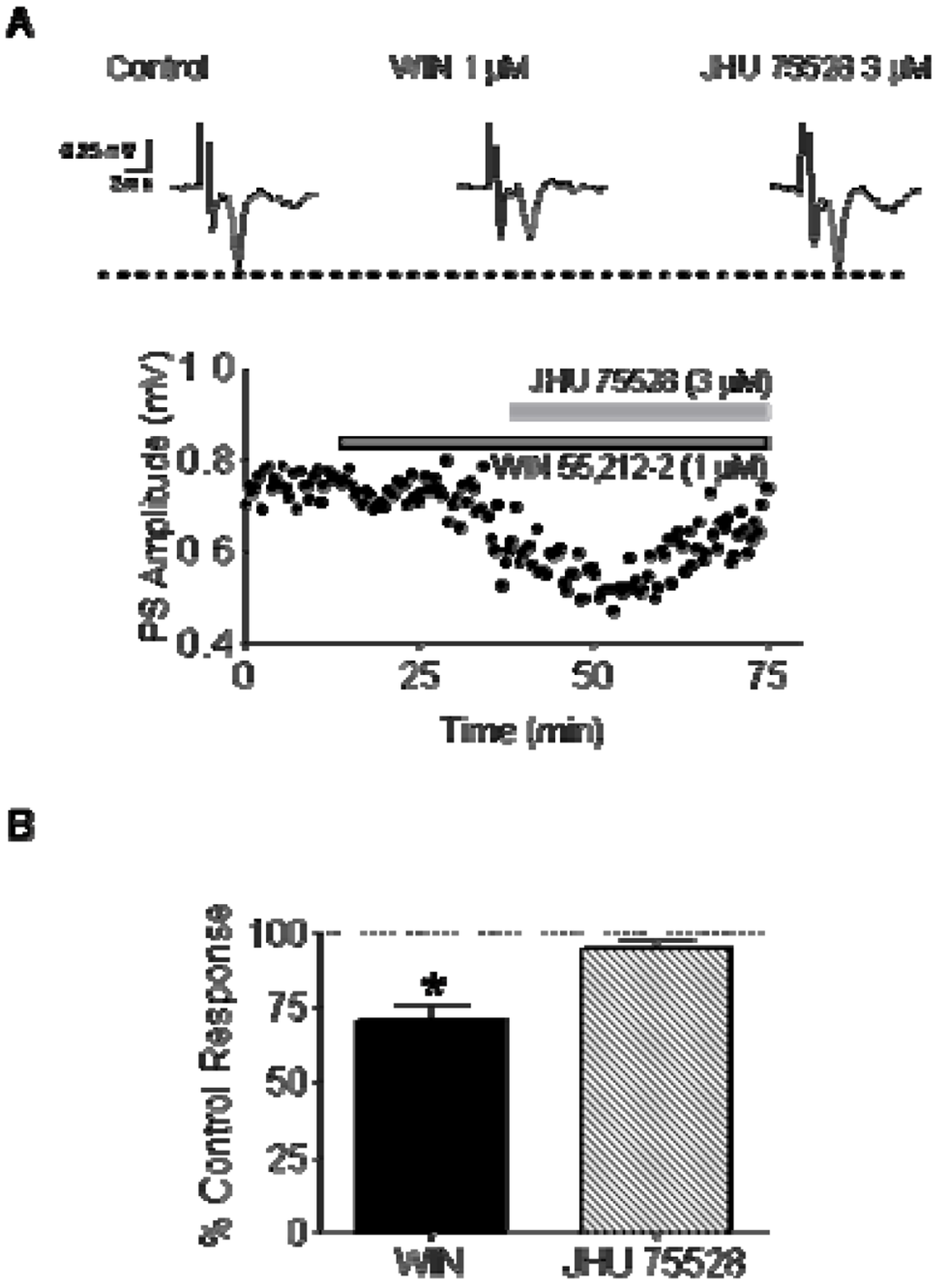

Figure 6.

Compound **4** (JHU75528) reverses the effects of the CB agonist WIN 55212-2 on glutamate release in striatal brain slices. (A) Extracellular recording of locally evoked, glutamatergic striatal population spikes (PS) were performed in mouse brain slices. Bath superfusion of 1 μM WIN 55212-2 produced a significant decrease in the PS amplitude, and this recovered to control (pre-drug) levels following superfusion with **4** (3 μM). (B) Summary of the reversal of WIN 55212-2 effects on glutamatergic responses by **4** in mouse brain slices (*$p < 0.05$, paired t-test, n = 5 slices from 3 animals). This confirms the CB antagonist properties of **4**.

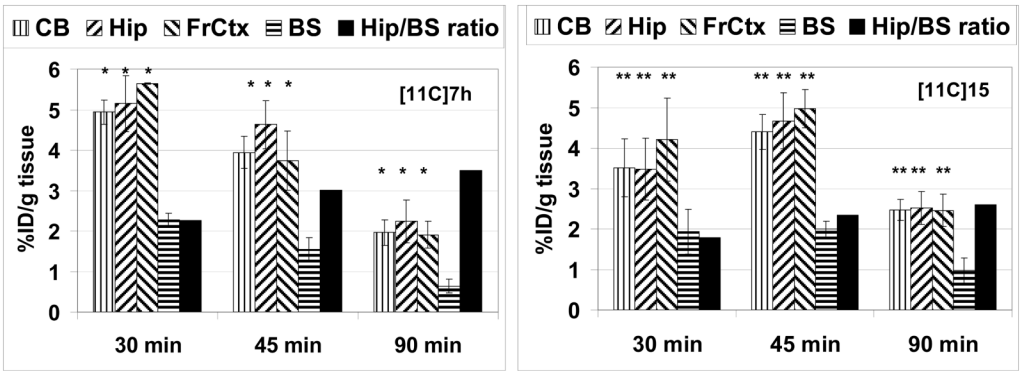

Figure 7.

Regional brain distribution of [^{11}C]**7h** (left) and [^{11}C]**15** (right) in CD-1 mice. CB = cerebellum; Hip = hippocampus; FrCtx = frontal cortex; BS = brain stem. Data are mean % ID/g tissue ± SD. Black bars are hippocampus/brainstem ratio. Data are mean ± SD. There was a significant difference between the uptake in brainstem and all other regions ([^{11}C]**7h**, **P*<0.03; [^{11}C]**15**, ***P*<0.05), data analysis is ANOVA single-factor.

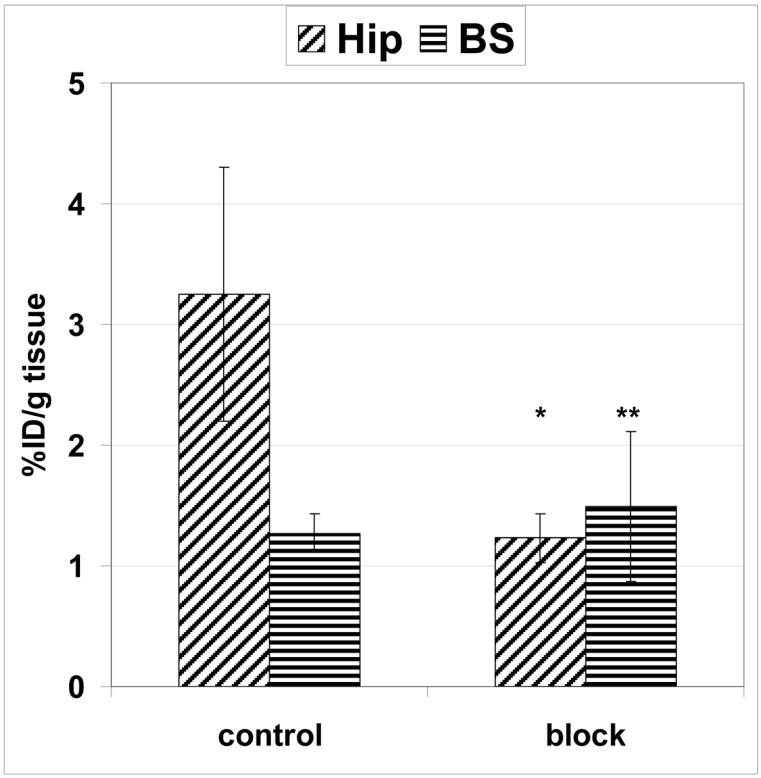

Figure 8.

Comparison of regional brain uptake (%ID/g tissue) of [^{11}C]**7h** in three CD-1 mice at 60 min time point in control and blocking experiments with Rimonabant **1** (1 mg/kg, i.v.). Data are mean ± SD. There was significant blocking in the hippocampus (Hip) (**P*=0.03). The blocking in the brainstem (BS) was insignificant (***P*=0.34). Data analysis is ANOVA single-factor.

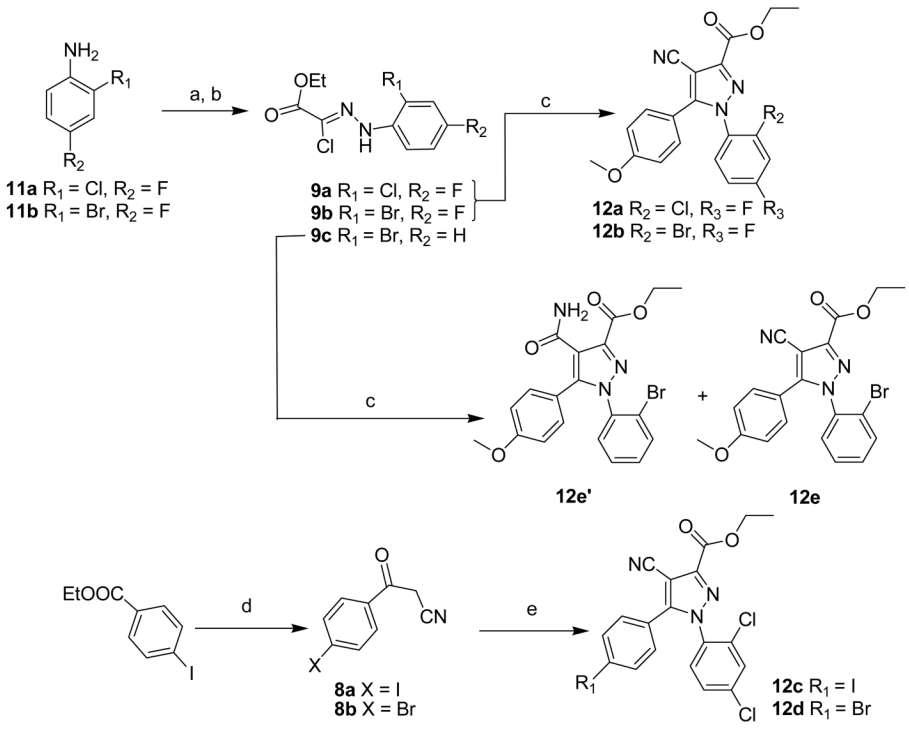

Scheme 1.

Reagents: (a) $NaNO_2$, HCl; (b) ethyl 2-chloro-acetoacetate, CH_3COONa, ethanol; (c) 4-methoxybezoylacetonitrile **8c**, sodium ethanolate; (d) sodium ethanolate, CH_3CN; (e) ethyl 2-chloro-2-(2-(2,4-dichlorophenyl)hydrazono)acetate **9d,** sodium ethanolate.

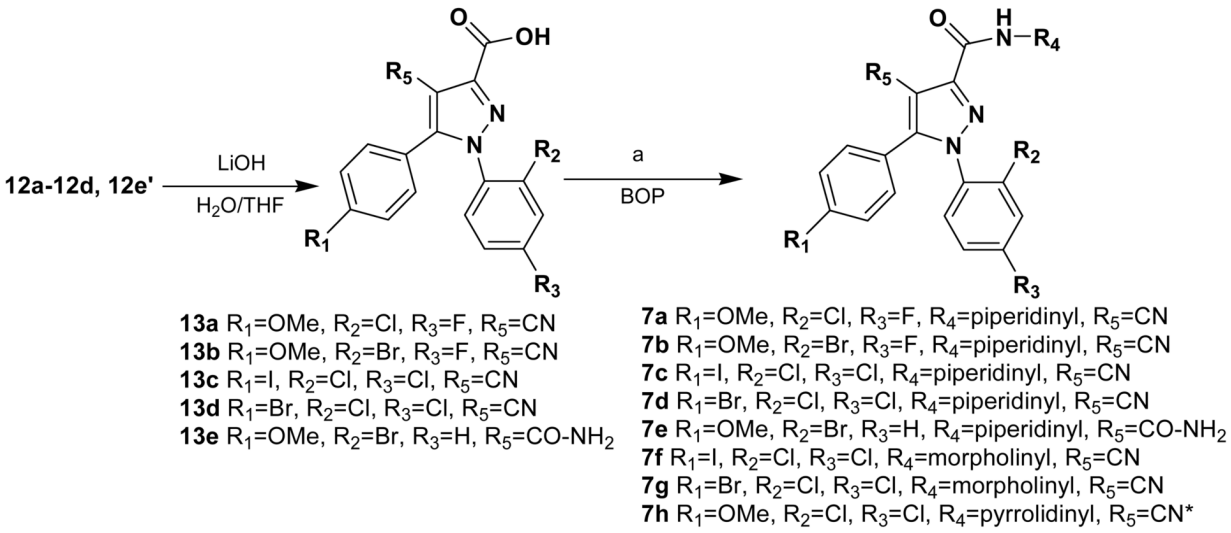

Scheme 2.

Reagents: BOP = Benzotriazol-1-yloxytris(dimethylamino)-phosphonium hexafluorophosphate, (a) N-aminopiperidine or N-aminomorpholine or N-aminopyrrolidine; * **7h** was prepared with 1-(2,4-dichlorophenyl)-4-cyano-5-(4-methoxyphenyl)-1*H*-pyrazole-3-carboxylic acid **13f** [31]

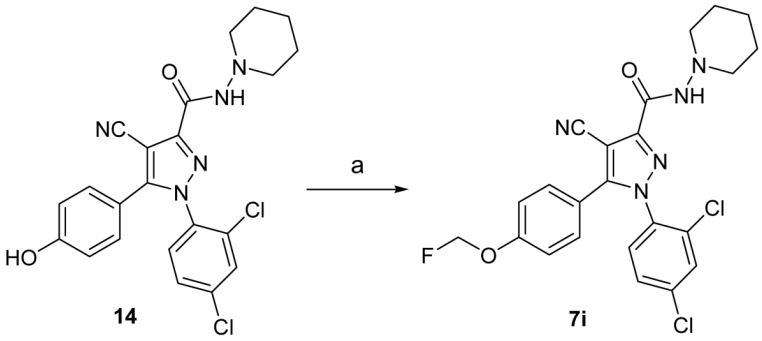

Scheme 3.
Reagents: (a) FCH_2OTs, K_2CO_3, acetone.

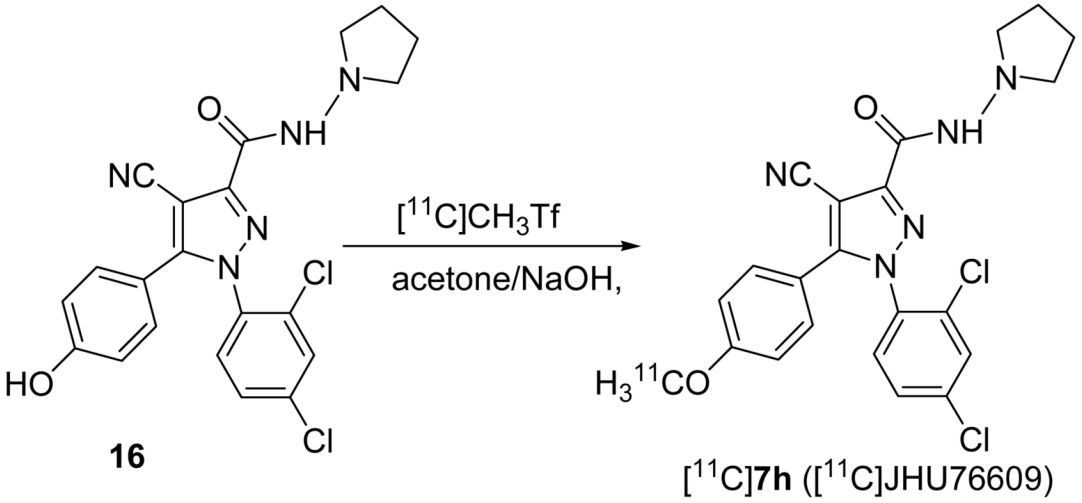

Scheme 4.
Radiosynthesis of [^{11}C]**7h** ([^{11}C]JHU76609).

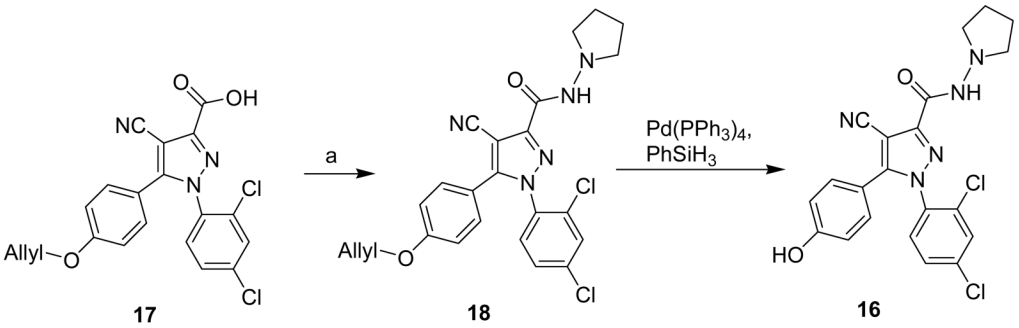

Scheme 5.

Synthesis of precursor **16** for radiolabeling of [^{11}C]**7h.** Reagents: [a]benzotriazol-1-yloxytris (dimethylamino)-phosphonium hexafluorophosphate (BOP), N-aminopyrrolidine.

Table 1

Comparison of inhibition binding affinity ([^{3}H]**2**, recombinant hCB1) and lipophilicity of compounds **1**, **2**, **4**, **15, 19** and **7a**–**7j**.

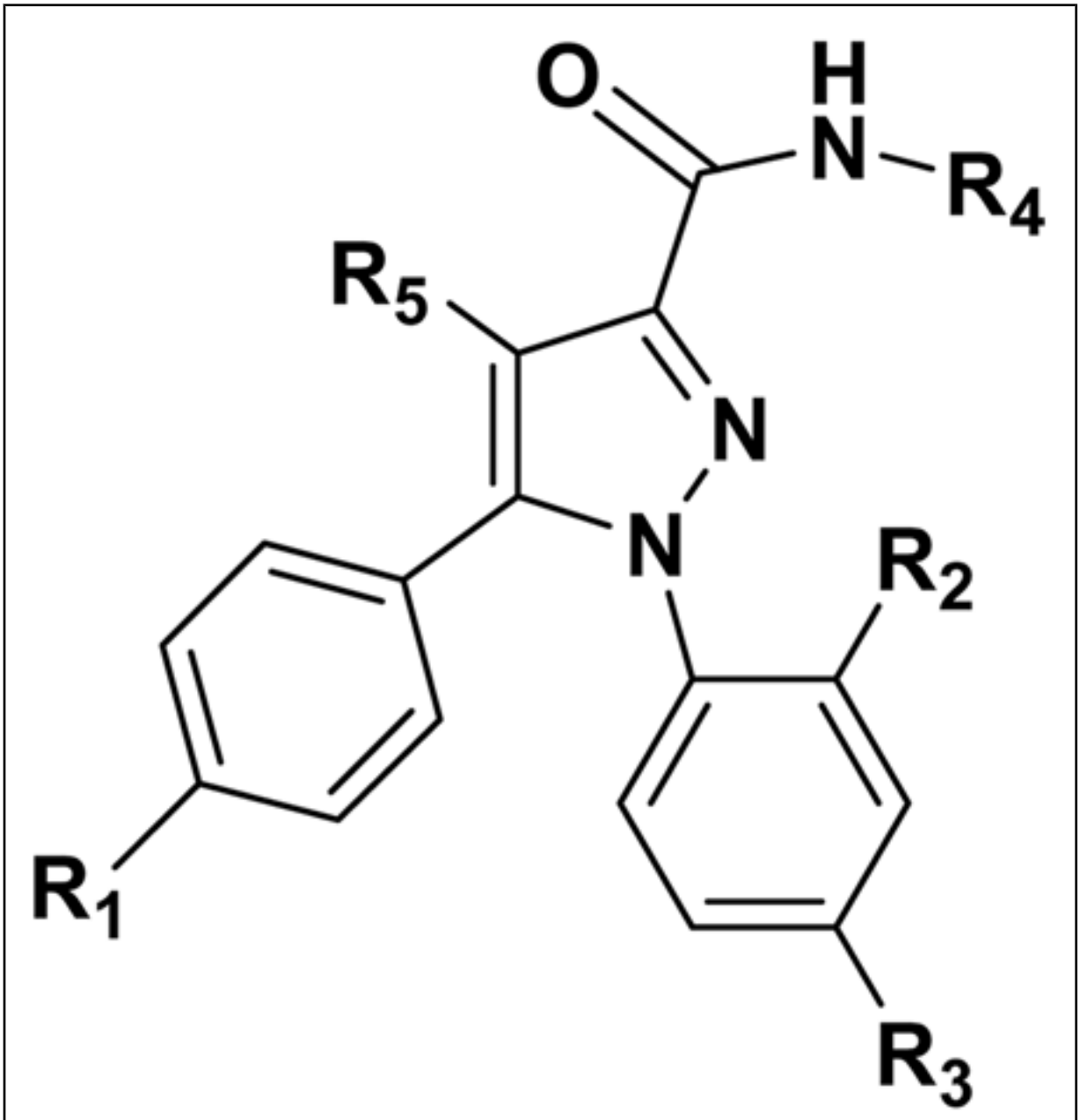

Compound	R_1	R_2	R_3	R_4[a]	R_5	Binding affinity, [b] K_i, nM	Experimental log$D_{7.4}$[c]
HU210	-	-	-	-	-	1.5 ± 0.8 (18)	-
1	Cl	Cl	Cl	Pip	CH_3	40 ± 8 (3)	4.6[31]
2	I	Cl	Cl	Mor	CH_3	422, 525[31]	-
4	OMe	Cl	Cl	Pip	CN	11 ± 7[31]	3.3–3.6[31]
15	OMe	Br	H	Pip	CN	4.7[31]	3.4[31]

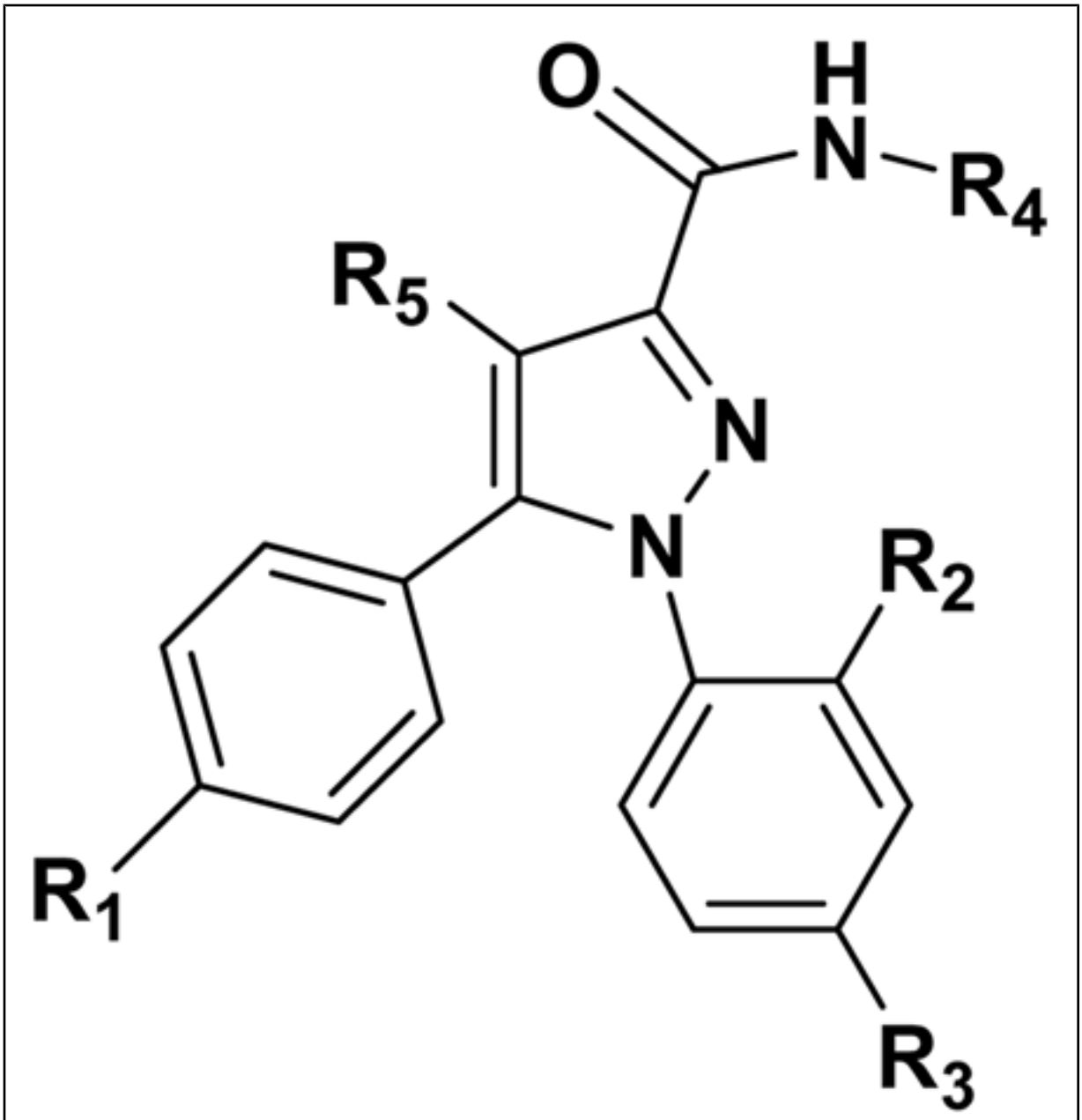

Compound	R_1	R_2	R_3	R_4[a]	R_5	Binding affinity, [b] K_i, nM	Experimental log$D_{7.4}$[c]
7a	OMe	Cl	F	Pip	CN	13, 18	2.8 ± 0.2(3)
7b	OMe	Br	F	Pip	CN	32, 37	2.9 ± 0.2(3)
7c	I	Cl	Cl	Pip	CN	33	3.9
7d	Br	Cl	Cl	Pip	CN	14, 20	3.7
7e	OMe	Br	H	Pip	NH_2CO	>10000	2.5
7f	I	Cl	Cl	Mor	CN	131	3.2
7g	Br	Cl	Cl	Mor	CN	>1000	3.1
7h	OMe	Cl	Cl	Pyr	CN	2.0, 3.7	2.8 ± 0.1(3)

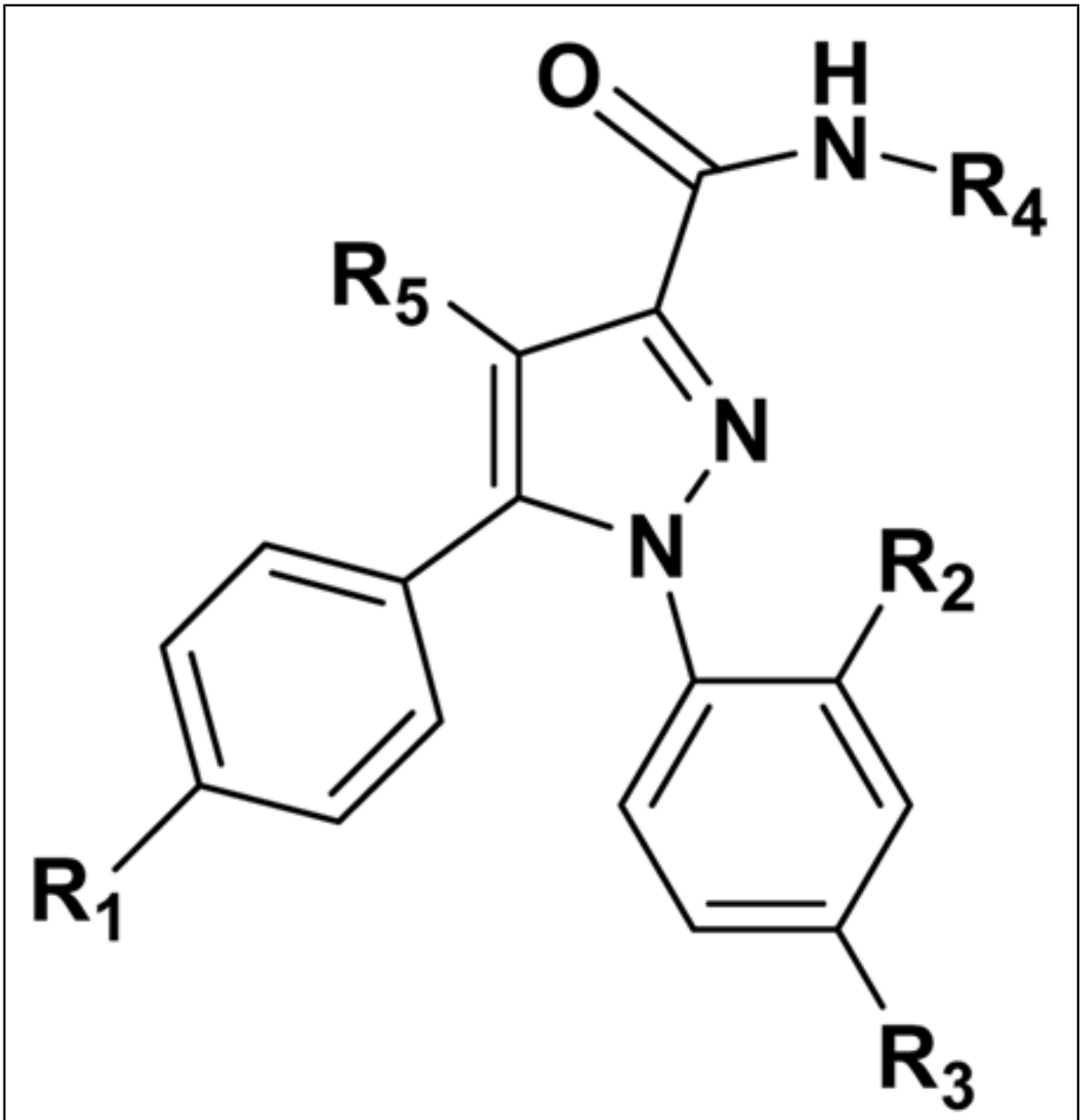

Compound	R_1	R_2	R_3	R_4[a]	R_5	Binding affinity, [b] K_i, nM	Experimental log$D_{7.4}$[c]
7i	OCH_2F	Cl	Cl	Pip	CN	10.3 ± 3.2 (3)	2.9 ± 0.3(3)
7j[d]	Cl	Cl	Cl	Pip	CN	24	3.5 ± 0.2(3)

[a] Pip=piperidinyl, Mor=morpholinyl, Pyr=pyrrolidinyl;

[b] Determination of inhibition binding affinity of all compounds in the Table have been done commercially by Novascreen under the same conditions as described,[31] K_i = mean ± S.D (number of independent assays), High affinity synthetic cannabinoid HU210[1,39] was used here as a reference standard;

[c] The octanol/phosphate buffer (pH=7.4) partition coefficients (log$D_{7.4}$) of compounds **7a-j** were measured using conventional flask-shake technique, mean ± S.D. (number of independent assays);

[d] Synthesized for this study as described elsewhere[35]

Table A1

Compounds 4 and 7e global minimum energy conformer measurements

Compound **7e** was found to have an intramolecular hydrogen bond between the C-4 carboxamide nitrogen and the C-3 carboxamide oxygen.

Substituent	Definition of torsion/angle/distance	Measurements	
		Compound 4	Compound 7e
C4 substituent	O-C1′-C3-C4	2.3°	−5.5°
Piperidine	LP-N3′-N2′-H	−1.0°	−1.7°
C5 substituent	C4-C5-C1‴-C2‴	−47.3°	−55.6°
Methoxy group	C3‴-C4‴-O-C	3.3°	3.2°
N1 substituent	N2-N1-C1″-C2″	−74.7°	−71.9°
HB distance	N--O	-	2.70Å
HB angle	N-H-O	-	156.0°

Table A2

Torsion changes of the docked compounds 4 and 7e

Compare to Table A1 above. The minimum energy conformer of **4** (lone pair pointing in the direction opposite to the carboxamide hydrogen; methoxy group flipped relative to global min; ΔE= 1.25 kcal/mol) was docked. Docking studies of **7e** also necessitated using the equivalent minimum energy conformer (lone pair pointing in the direction opposite to the carboxamide hydrogen and methoxy group flipped; ΔE= 1.25 kcal/mol).

Substituent	Definition of torsion/angle/distance	Measurements	
		Compound 4	Compound 7e
Piperidine	LP-N3′-N2′-H	178.8°	179.5°
Methoxy group	C3‴-C4‴-O-C	−165.1°	177.1°

Table A3

Pair-wise Interaction Energies for **4** and **1** with CB1 R Binding Pocket Residues, Conformational Energy Expense for Each Ligand Dock and the Combined Energy for Each Ligand/CB1 R Complex.

	Compound 4		Compound 1	
Residues	**Coulomb (kJ/mol)**	**vdW (kJ/mol)**	**Coulomb (kJ/mol)**	**vdW (kJ/mol)**
K3.28	−92.84	−3.34	−72.02	−8.81
L3.29	−2.26	−13.49	0.53	−9.99
V3.32	0.71	−14.14	−1.04	−20.29
T3.33	−0.23	−4.78	−1.29	−11.01
F3.36	−4.32	−14.47	−1.11	−14.39
T3.37	0.05	−0.28	0.02	−2.86
I4.56	0.07	−0.46	−0.74	−3.61
Y5.39	−3.32	−6.69	−1.02	−6.59
W5.43	−1.41	−29.34	−0.70	−25.10
W6.48	−0.22	−0.76	−0.31	−0.84
I6.54	0.26	−5.21	0.25	−3.13
M6.55	1.48	−32.22	2.49	−28.36
D6.58	3.31	−15.72	5.67	−6.75
F7.35	−2.20	−9.98	−0.12	−1.03
C7.38	0.23	−5.28	−0.24	−0.61
S7.39	0.08	−4.81	−0.85	−5.75
C7.42	−0.65	−5.06	1.71	−6.03
SubTotal (kJ/mol)	−101.27	−166.03	−68.77	−155.14
SubTotal (kcal/mol)	−24.19	−39.66	−16.43	−37.05
Total (kJ/mol)	−267.30		−223.91	
Total (kcal/mol)	−63.84		−53.48	
Ligand Conf. Cost* (kcal/mol)	1.29		1.26	
Combined Total (kcal/mol)	−62.55		−52.22	

Energy calculated at the HF-6-31G level (see Experimental Section).